AFAMRL-TR-80-134

EFFECTS ON TARGET TRACKING OF MOTION SIMULATOR DRIVE-LOGIC FILTERS

HENRY R. JEX
RAYMOND E. MAGDALENO
WAYNE F. JEWELL

SYSTEMS TECHNOLOGY, INC.
13766 SOUTH HAWTHORNE BOULEVARD
HAWTHORNE, CALIFORNIA 90250

ANDREW JUNKER
GRANT McMILLAN

AIR FORCE AEROSPACE MEDICAL RESEARCH LABORATORY

OCTOBER 1981

Approved for public release; distribution unlimited

AIR FORCE AEROSPACE MEDICAL RESEARCH LABORATORY
AEROSPACE MEDICAL DIVISION
AIR FORCE SYSTEMS COMMAND
WRIGHT-PATTERSON AIR FORCE BASE, OHIO 45433

NOTICES

When US Government drawings, specifications, or other data are used for any purpose other than a definitely related Government procurement operation, the Government hereby incurs no responsibility nor any obligation whatsoever, and the fact that the Government may have formulated, furnished, or in any way supplied the said drawings, specifications, or other data, is not to be regarded by implication or otherwise, as in any manner licensing the holder or any other person or corporation, or conveying any rights or permission to manufacture, use, or sell any patented invention that may in any way be related thereto.

Please do not request copies of this report from Air Force Aerospace Medical Research Laboratory. Additional copies may be purchased from:

National Technical Information Service
5285 Port Royal Road
Springfield, Virginia 22161

Federal Government agencies and their contractors registered with Defense Documentation Center should direct requests for copies of this report to:

Defense Documentation Center
Cameron Station
Alexandria, Virginia 22314

TECHNICAL REVIEW AND APPROVAL

AFAMRL-TR-80-134

This report has been reviewed by the Office of Public Affairs (PA) and is releasable to the National Technical Information Service (NTIS). At NTIS, it will be available to the general public, including foreign nations.

This technical report has been reviewed and is approved for publication.

FOR THE COMMANDER

CHARLES BATES, JR.
Chief
Human Engineering Division
Air Force Aerospace Medical Research Laboratory

SECURITY CLASSIFICATION OF THIS PAGE *(When Data Entered)*

REPORT DOCUMENTATION PAGE

READ INSTRUCTIONS BEFORE COMPLETING FORM

1. REPORT NUMBER: AFAMRL-TR-80-134	2. GOVT ACCESSION NO.
3. RECIPIENT'S CATALOG NUMBER	
4. TITLE *(and Subtitle)*: EFFECTS ON TARGET TRACKING OF MOTION SIMULATOR DRIVE-LOGIC FILTERS	5. TYPE OF REPORT & PERIOD COVERED: Final Report
	6. PERFORMING ORG. REPORT NUMBER: STI-TR-1094-1
7. AUTHOR(s): Henry R. Jex, Raymond E. Magdaleno, Wayne F. Jewell, Andrew Junker*, Grant McMillan*	8. CONTRACT OR GRANT NUMBER(s): F33615-77-C-0508
9. PERFORMING ORGANIZATION NAME AND ADDRESS: Systems Technology, Inc., 13766 South Hawthorne Boulevard, Hawthorne, California 90250	10. PROGRAM ELEMENT, PROJECT, TASK AREA & WORK UNIT NUMBERS: 62202F, 6893-06-02
11. CONTROLLING OFFICE NAME AND ADDRESS: Air Force Aerospace Medical Research Laboratory, Aerospace Medical Division, AFSC, Wright-Patterson Air Force Base, OH 45433	12. REPORT DATE: October 1981
	13. NUMBER OF PAGES: 92
14. MONITORING AGENCY NAME & ADDRESS *(if different from Controlling Office)*	15. SECURITY CLASS. *(of this report)*: Unclassified
	15a. DECLASSIFICATION DOWNGRADING SCHEDULE

16. DISTRIBUTION STATEMENT *(of this Report)*

Approved for public release; distribution unlimited.

17. DISTRIBUTION STATEMENT *(of the abstract entered in Block 20, if different from Report)*

18. SUPPLEMENTARY NOTES

*Crew Systems Effectiveness Branch
Human Engineering Division
Air Force Aerospace Medical Research Laboratory

19. KEY WORDS *(Continue on reverse side if necessary and identify by block number)*

Pilot performance
Motion cueing
Motion washout
Roll axis motion
Sway axis motion
Roll tilt cue

20. ABSTRACT *(Continue on reverse side if necessary and identify by block number)*

Two experiments were performed on separate moving-base flight simulators at Wright-Patterson AFB to determine the effects on air-to-air tracking tasks of motion-reducing drive logic (washout filters) in the roll and sway degrees-of freedom. Measurements included not only error and control performance, but also pilot behavior (describing functions and fitted parameters) and pilot subjective evaluations. Excellent consistency of data resulted across the two

(Continued)

DD FORM 1 JAN 73 1473 EDITION OF 1 NOV 65 IS OBSOLETE

SECURITY CLASSIFICATION OF THIS PAGE *(When Data Entered)*

20. ABSTRACT (Cont'd)

facilities, and between very thoroughly practiced non-pilots and experienced military pilots. The results indicate that rotary motion cues are used primarily in the role of stability augmenters (i.e., as rate dampers) and that lateral specific-force cues below 0.1 G_y are ignored or have small effects. Limited data indicate that grossly spurious motion distortion due to washout filter dynamics were rated and performed worse than no motion at all. Optimum combinations of attenuation and first-order washout filtering were found for the roll-motion drive logic. An adaptive nonlinear logic was developed and validated for the sway drive logic.

SUMMARY

Two closely related experiments were performed on moving-base simulators to investigate the effects on pilot tracking performance and dynamic behavior of various types of motion-reducing drive logic (washout filters). The basic piloting task was to follow an evasive (randomly rolling) target while suppressing gust disturbances due to its wake. A dual-input technique produced behavioral data (describing functions) and performance data (error and control scores), which revealed how pilots used the visual and motion cues. Subjective data were also gathered on the realism of the resulting motion cues.

Experiment I was performed on the AFAMRL Dynamic Environment Simulator (DES) in the roll degree of freedom only. To investigate tilt cue effects the G vector was oriented either normally (pilot erect, tilt cue present) or 90 degrees nose-up (pilot supine, no tilt cue). The experiment included using full motion and the following washout filter conditions: second- and first-order, attenuated first-order, attenuated, and static (fixed-base). Four non-military-pilot subjects were carefully trained to asymptotic performance, and all showed remarkably consistent describing functions, and similar error and control scores. It was clearly shown that the roll-rate motion cues helped the subjects to resist gust disturbances, but that they had small effects on target tracking errors. The describing functions showed that tilt cues were used when available to stabilize low-frequency motions, but that they gave only small improvements in error scores. The optimum roll-only drive logic (with respect to achieving full-motion-like flight control behavior, reduced roll movements, and acceptable motion cue fidelity) was the combined attenuation and first-order filter condition.

Experiment II, using the same task and dynamics as Experiment I, was performed in the Large Amplitude Multimode Aerospace Research Simulator (LAMARS) of the Flight Dynamics Laboratory. The objectives were to: a) compare the roll-only results on LAMARS, using four experienced

fighter pilots, with the nonpilot results on the DES; and b) investigate the degree to which the spurious G-vector tilt cue can be coordinated out by limited sway axis motion. The large lateral aircraft motions which would normally result from rolling maneuvers were reduced by high-pass sway washout filters of second-order form with adjustable break frequency, ω_y; damping ratio, $\zeta_y = 0.7$; and adjustable attenuation factor, K_y. A range of K_y and ω_y was explored, from which example data are shown. A nonlinear (adaptive time varying) washout was developed and tested wherein ω_y was continuously adjusted so as to permit correct cues for small roll activity, while reducing the travel peaks for large roll angles. Reshaping the forcing functions was also investigated. The results of Experiment II showed: a) excellent agreement with the Experiment I data from non-pilot subjects; b) most tracking performance and behavioral parameters were not significantly affected by various degrees of sway washout; c) pilot commentary became more consistent and adverse as the spurious side-force peaks exceeded about 0.1 G_y; and d) a mapping of specific problems as a function of ω_y vs. K_y. The Experiment II results imply that: a) non-pilots can be used in motion cue research, provided they are trained very thoroughly; and b) that almost any translational washout that keeps flight simulator motions within ±10 ft or less will have annoyingly unrealistic motion or artifacts when large maneuvers are simulated.

PREFACE

This report concludes a project to improve the validity of flight motion simulation. The usefulness of motion simulation is hindered by the necessary limits on travel. These limits are provided by drive-logic "washout filters", generally selected from motion limiting considerations at the expense of distorted motion cues. The approach taken here was to seek the optimum drive logic which would reduce the motions to a prescribed amount while preserving the pilot/vehicle tracking performance and achieving realistic pilot dynamic behavior.

The research was performed jointly by the Air Force Aerospace Medical Research Laboratory (AMRL) at Wright-Patterson AFB (the sponsor) and by Systems Technology, Inc. (STI) under Contract F33615-77-C-0508. The AMRL provided the test facilities and tracking apparatus as well as the pilots. It also performed raw data collection and reduction, and test support at all levels, including portions of the report. STI helped AMRL to design the experiments and it developed the various test conditions and tracking tasks, models and parameters, provided test assistance, analyzed and interpreted the results, and prepared most of the report.

The AMRL personnel were Andrew Junker, who initiated the research, executed Experiment I, and planned Experiment II; and Grant McMillan, who made significant contributions to Experiment II and the final report. The principal STI investigators were Henry Jex and Raymond Magdaleno, at all stages, with contributions from John Sinacori in the planning stages and Wayne Jewell during Experiment II, who also developed the nonlinear sway filter scheme tested herein. Thanks are due to the exceptional support given by Marvin Rourke (then at Systems Research Lab.) for the software to run the experiments, and to Jim Ater and Warren Miller (then at AMRL) for smooth test operations. In the spirit of collaborative research, the AF Flight Dynamics Branch's LAMARS facility was made available for Experiment II of this AMRL project by Paul Blatt, and creative support was provided there by John Bankovskis and the LAMARS operating staff. Finally, we all appreciate the dogged devotion of the four anonymous non-pilots (who practiced for weeks to achieve pilot-quality performance) and the four anonymous military pilots at Wright Patterson AFB who found time to fit several days of simulation runs among their otherwise busy schedules.

TABLE OF CONTENTS

LIST OF ILLUSTRATIONS

LIST OF TABLES

INTRODUCTION AND BACKGROUND

Motion cues are often used in flight simulators in the hope of enhancing the realism and validity of results with respect to free flight. However, mechanical and cost constraints usually limit the amount of rotary or translational motion that can be achieved. Various types of drive logic (washout filters) are used between the computed aircraft motions and the simulator servo drives to keep the motions within these constraints. These filters may distort the amplitude or timing of motion cues compared to flight and, thereby, introduce simulation artifacts which lessen the realism and distort the motion cues sufficiently to reduce the validity of moving-base simulation. Because moving-base simulators are expensive to acquire and operate, and because their use in training applications must not result in a student being trained to use the wrong cues, motion drive logic must be carefully optimized to achieve a balance between realistic pilot/vehicle behavior and large reductions in the true physical motions.

As part of a long-term research program on the basic effects and optimization of motion simulator drive logic, the Air Force Aerospace Medical Research Laboratory (AFAMRL) conducted two related experiments on separate facilities at Wright-Patterson AFB (WPAFB):

- Experiment I was performed on the AFAMRL Dynamic Environment Simulator (DES) in only the roll degree of freedom to investigate the effects of G-vector tilt cues and various types of washout filters.

- Experiment II, using the same task and vehicle dynamics as Experiment I, was performed in the Large Amplitude Multimode Aerospace Research Simulator (LAMARS) at the Flight Dynamics Lab (FDL) in both roll and sway degrees of freedom to investigate the degree to which the G-vector tilt cue could be coordinated out, as in flight, by limited sway motions from various filter combinations. In addition, experienced military pilots were used in Experiment II, to tie in results with the Experiment I well-trained nonpilots.

Because both experiments used common tasks and analysis procedures and were progressive in experimental design, both are discussed in this report. However, each was performed separately in time and facilities, so each is covered by separate portions of this report.

EXPERIMENT I — PURE ROLL MOTIONS AND G-VECTOR TILT

OBJECTIVES

Experiment I was conducted to define a pilot's use of motion cues in moving-base simulators free to rotate only in the roll degree of freedom. This situation provides the pilot an intrinsically spurious roll attitude or "tilt" cue. This effect can be reduced by "washing out" the cab motion so the cab always tends to return to an upright orientation, although this distorts the true angular rate motions. The optimization of the washout filter to achieve the best compromise between realistic roll rate cues and suppression of the spurious tilt cue is an important facet of the ongoing research in the Dynamic Environment Simulator, which is limited to pure roll and pitch motions at various steady G-levels.

The basic objective was to determine what form and degree of washout dynamics achieves the highest simulation realism, while engendering true-to-life behavior of the pilot, and producing the correct performance effects due to environmental stressors. Longer range objectives include the possible correlation of these experiments with other ground-based simulations and, later, with in-flight experiments.

To accomplish the above objectives this investigation had to consider two basic problems in moving-base simulation: the use of motion cues by the pilot in the actual ("real world") case and the effects of spurious motion cues in modifying that usage in the simulator. A brief examination of the piloting task involved in the first problem is useful before proceeding to the second.

Consider a situation of primary interest to the Air Force--air-to-air combat--and focus upon the pilot's response to the dynamic (non-steady) components of motion. Assume that, initially, the pilot has his wings lined up with those of a target aircraft that he perceives against

a murky or nighttime background (no horizon visible). In this "impoverished display" situation he can visually perceive only the difference (error) between the target's wings and his own. Further, the pilot has two tasks to perform, often simultaneously:

a) Regulate (suppress) disturbances, e.g., due to turbulence from the target's wingtip vortices. In this task the pilot's role is to reduce motions, and if he suppresses the gusts well the physical motions become smaller.

b) Track (follow) the target roll motions (e.g., by keeping one's wings parallel with the target). In this task the pilot's role is to reproduce motions, and if he tracks well, the physical motions become larger (i.e., they approach the target motions).

In an operational environment where both inputs are present, the pilot is faced with a continual conflict between suppressing disturbance motions and following the target motions. The figure-of-merit (at least in air combat and landing tasks) is primarily low roll error (and, perhaps, limited roll acceleration or its rough equivalent, aileron control deflection). Because multiple sensory feedbacks are involved, with more than one input, the problem is a multiloop one, and this greatly complicates the control system analysis, as well as the attempt to infer the pilot's behavioral strategy (loop structure) and parameters, as will be demonstrated.

Most of the earlier research in measuring the use of visual and motion cues, such as that of Shirley (1968) and Stapleford et al. (1969) tended to make either the target or disturbance input as dominant, such that the possible cue conflicts were minimized. Stapleford et al., were able to infer the separate visual and motion pathway dynamics by using mathematically independent target and disturbance inputs comprising sums of sinusoids interleaved in frequency and then interpolating between frequencies to solve the simultaneous vector equations required to untangle the loops (this process will be shown later herein). However, these pioneering results were not fitted in any model form suitable for efficient use. Thus, the secondary objectives of this program were to

improve the reduction and analysis of multisensory manual control data, and to structure and model the results. Here, where the target following and disturbance motions were comparable, in bandwidth and amplitude, new techniques were required.

Such a situation seems natural for an optimal control model of the human operator; and Levison et al. (1976, 1977), working with AMRL experimenters, have put forth a first cut at just such a model. The forcing functions were either target inputs or disturbances, and effects similar to Stapleford's and Shirley's were obtained. Whether or not their (implicitly) assumed feedback structure is generally valid is hard to say without more data on the all-important dual-input case treated here.

In another approach Zacharias and Young (1977) have addressed the problem of sensory conflict of visual and vestibular sensors in conjunction with regulation of purely visual, purely motion, or conflicting cue situations, and have suggested a cue-conflict-resolving model for the human operator in the yaw-only degree of freedom. Testing the validity of such cue-conflict-resolution approaches as these requires a very solid data base against which to exercise one's model against, and this is still largely lacking. In light of the above needs, a third objective was to establish a very solid and comprehensive data base, using inputs, controlled elements, and washouts that were analytically tractable and fairly linear, so that future validation of cue-utilization models would be facilitated.

APPROACH

As noted above, there were two facets of roll motion cue usage to be investigated: "real-world" motion versus no motion and distortions of real-world motion by various washout filters. In actual flight, where bank angles result in lateral acceleration of the aircraft, there is no lateral specific force. Thus, haptic or vestibular sensors cannot be used to detect the true vertical. A set of realistic rolling cues was simulated by tipping the roll axis of the DES 90 deg nose upward so that

the spurious tilt cues were absent. This "full motion at 90 deg inclined roll axis" (F90) case was given the most practice and became the "real-world" reference for all other motion cases. By comparing it with the static case, the basic effects of full rolling motion were revealed. To check effects of the conflicts between target following versus disturbance regulation, both forcing functions were given alone and together (dual input) for the F90 case. If the dual case gave similar data to either input alone, then the dual input could be used throughout, with consequent savings in runs and data analysis.

Motion washouts in roll-only simulators are used for two main purposes:

a) To reduce the tilt cues (largely a low frequency effect).

b) To reduce any or all motions (accelerations, rates, displacements) to fit into a limited capability simulator, always with a horizontal orientation of the roll axis.

Consequently the effects of simulated roll-only motions were covered by the full motion at 0 deg roll axis inclination (F0 case), plus various washouts — all selected to give substantial reduction in roll displacement.

To keep the number of runs within bounds, we decided to keep the plant and the spectra of forcing functions constant, and to investigate only one variation of each washout filter scheme. Each washout was selected originally from a simplified scheme to give a comparable factor of motion attenuation.

METHOD

Experimental Conditions

Control Task

A scenario with high relevance to Air Force problems is air-to-air gunnery. In a modern high thrust-to-weight fighter, combat maneuvers take place at all flight path angles, hence the horizon is relatively

unimportant. The main criterion for an accurate tail chase is to match the roll angle of the target aircraft. The pilot is attempting to follow an evasive target while at the same time he may be buffeted by turbulence from the wing tip vortices of the target. To simplify the simulation and subsequent modeling and interpretation, a compensatory display (error only) was used and the subjects were instructed to minimize the bank angle error.

Figure 1a illustrates the basic elements involved: the Human Operator, Controlled Element, and Washout Dynamics. The multiloop piloting task is evident in that the Motion Response responds to physical (inertial) bank angle while the Visual Response responds to the displayed error between target and task bank angle.

Controlled Element

In the actual mechanization the computer portion of the controlled element is followed by the washout filter that drives the DES motion system. For convenience, and without loss of accuracy, the first and last items are combined into the controlled element dynamics, followed by the washout filter. The controlled element (Eq. 1 on Figure 1b) represents an approximation to the roll dynamics of a fighter. The Roll Subsidence mode, having a time constant of $1/1.6 = 0.63$ sec, is typical of a loaded fighter (i.e., with external stores). This value was selected as it would require a significant amount of lead generation by the pilot, as predicted by the Crossover Law for human operator equalization (e.g., McRuer and Krendel, 1974). In such cases the ideal pilot lead would be about 0.5-0.7 sec. The "Structural Mode" and "DES Lags" represent the unavoidable (measured) response characteristics of the DES motion simulator, while the "Servo Lag" represents actuation lags of a (poor) aircraft control system. It was raised to 0.2 sec to prevent excessive acceleration or rate commands to the DES, which would cause its drives to operate in a partly saturated (hence nonlinear) manner.

Analysis of this controlled element showed that it required a fairly tightly constrained pilot equalization, with some lead to offset the roll-subsidence lag, but not too much or else the structural mode and

a. Block Diagram Showing Definitions of Elements and Signals

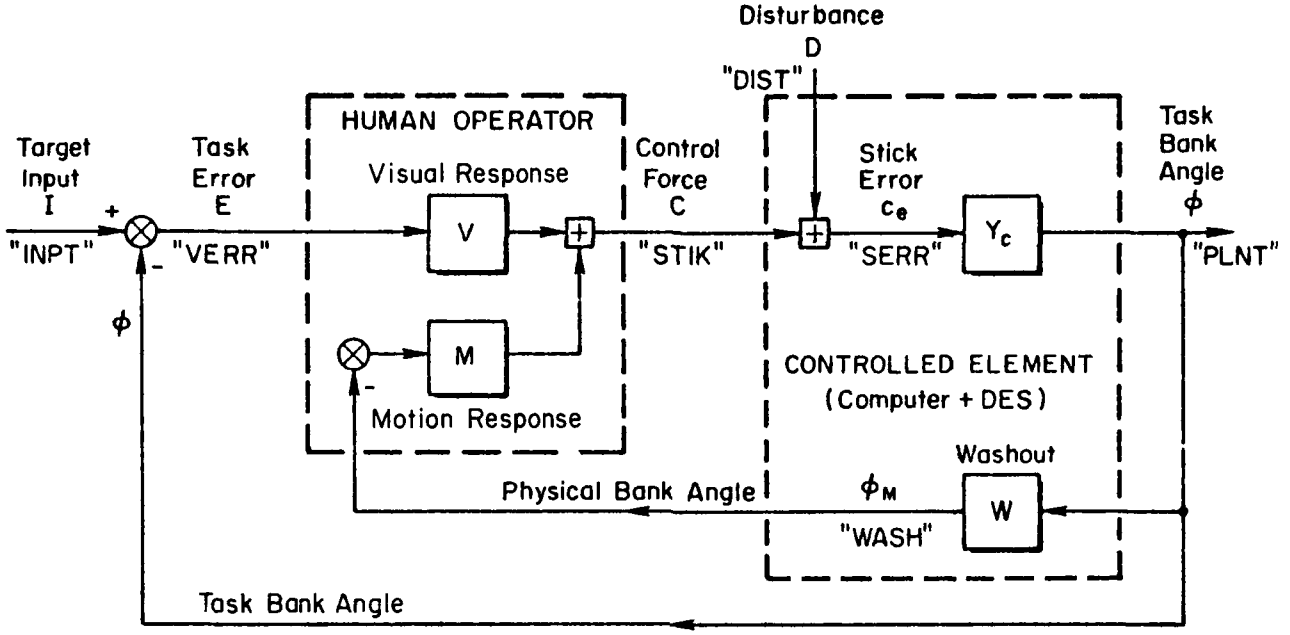

Note: "---" denotes signal names in data reduction

b. Controlled Element Transfer Function

$$Y_c(s) \equiv \frac{\varphi}{c_e} \doteq 17 \; \frac{\overbrace{(-s/25 + 1)}^{\text{DES Lags}}}{\underbrace{s}_{\text{Spiral Mode}} \; \underbrace{\left(\frac{s}{1.6} + 1\right)}_{\text{Roll Subsidence}} \; \underbrace{\left(\frac{s}{5} + 1\right)}_{\text{"Servo" Lag}} \; \underbrace{\left[\frac{s^2}{11^2} + \frac{2(.3)s}{11} + 1\right]}_{\text{"Structural" Mode}}} \; ; \; \left(\frac{\text{deg/sec}}{\text{lb}}\right) \qquad (1)$$

In Computer | In Dynamic Environment Simulator

In ST units the static gain is 3.8 $\frac{\text{deg/sec}}{\text{N}}$ or .067 $\frac{\text{rad/sec}}{\text{N}}$

Figure 1. Roll Tracking Task Block Diagram and Transfer Function

lag elements would destabilize the system. Thus, there was a clearly optimum control strategy for the subjects to learn; this was important because they were not experienced pilots.

Forcing Functions

Quasi-random target and disturbance inputs were constructed from eight sinusoids each (Table 1). The frequencies were selected so as to have an integer number of cycles in the run length. To assure statistically independent inputs, target and disturbance frequencies were interleaved, yet each was approximately evenly spaced on a log-frequency plot. After these choices were made the amplitudes were "shaped" to simulate a random noise process that would result from white noise being filtered by the shaping filter forms given in Table 1. Finally, these "shaped amplitudes" were uniformly scaled so as to give the listed rms and peak amplitude values.

The target's shaping filter was selected to simulate a low pass spectrum typical of an evasive target. The disturbance's shaping filter was selected so that under static conditions (and, as further shaped by the controlled element) the spectral content and rms values would be nearly equal to that of the target, as seen on the error display. Thus the pilot could not use either input's statistical properties to separate target motions from disturbance motions.

Washout Dynamics

In addition to the "Static" (no motion) case (ST) and Full Motion cases with roll axis at 0 deg inclination (F0) and nose up 90 deg (F90), four different washout logics were tested:

TABLE 1. FORCING FUNCTIONS FOR DUAL INPUT RUNS

TARGET (rms = 7.1 deg)*			DISTURBANCE (rms = .74 lb = 3.4 N)*		
Cycles / Run Length†	ω (rad/sec)	A_{dB} 0 = 1. deg	Cycles / Run Length	ω (rad/sec)	A_{dB} 0 = 1. lb
5	0.19	13.6	9	0.35	−20.6
12	0.50	11.6	17	0.65	−16.5
23	0.88	8.7	30	1.15	−13.6
37	1.42	5.6	49	1.88	−11.4
63	2.42	1.0	83	3.18	− 9.7
107	4.10	− 5.8	141	5.41	− 9.2
182	6.98	−14.4	241	9.24	−10.0
309	11.85	−24.4	410	15.72	−11.7
SHAPING FILTER FORMS					
$\frac{1}{(s+0.5)(s+1.7)(s+5.0)}$			$\frac{s}{(s+0.5)(s+5.)}$		

* For single input runs the values were increased by $\sqrt{2}:1 = 1.41$
† Run length = 163.84 sec = 2.73 minutes

Case A "Purely Attenuated," wherein the plant motions at all frequencies were multiplied by 0.5 in commanding the DES.

Case W1 "First Order," where the low frequency motions are attenuated by a first-order high pass filter of the form

$$\left.\frac{\phi_M}{\phi}\right|_{W1} = \frac{K_{hi}s}{s + 1/T} \tag{2}$$

where

K_{hi} = High frequency gain (near 1.0)

T = Time constant ("break frequency" = $1/T$)

With this washout a step bank angle command returns exponentially to zero with a time constant of T sec.

Case W1A "First-Order, Attenuated," a combination of the two foregoing washouts, with different gains and break frequencies.

Case W2 "Second-Order," the low frequency terms are washed out by second-order high pass filter of the form

$$\left.\frac{\phi_M}{\phi}\right|_{W2} = \frac{K_{hi}s^2}{s^2 + 2\zeta\omega s + \omega^2} \tag{3}$$

where

K_{hi} = High frequency gain (near 1.0)

ω = Break frequency

ζ = Damping ratio (typically 0.7)

With such a second-order washout an initial step bank angle returns with minimal overshoot with an effective delay (to half amplitude) of $2\zeta/\omega$ sec. A constant roll rate input still ends up at zero bank angle.

The various washout parameters were originally selected to produce a reduction in rms roll amplitude to about 50 percent of the full motion case, based on a more or less arbitrary a priori assumption of a typical, invariant, second-order closed-loop pilot-simulator response to roll commands, characterized by a bandwidth of 3.6 rad/sec and a closed-loop damping ratio of $\zeta_{CL} \triangleq 0.6$. We realized that, in practice, the

pilot might change his response characteristics for different washouts, but this procedure was used to select the different parameters on a more rational basis than (say) fixed break frequencies of all the washouts. No attempt was made to account for the changes in pilot behavior with changes in washout.

In the simulation, problems with mechanization of the filters and DES response properties slightly modified the intended washout dynamics. The actual response properties of the washout plus DES combination were fitted by the appropriate forms of Eqs. 2 and 3 and the effective washout-filter parameters were extracted. These are summarized in Table 2. Most of the effective parameters were close to the intended ones, except for the W2 high frequency gain, which was 1.2 instead of the 1.0 desired. In Table 2 the cases are arranged in order of decreasing magnitude of rms physical roll angle, and this order will be used throughout the presentations to follow.

TABLE 2. MOTION CONDITIONS AND MEASURED WASHOUT DYNAMICS

CASE	WASHOUT TYPE	HIGH FREQUENCY GAIN	BREAK
F90	"Full Motion" at 90 deg	1.0	--
F0	"Full Motion" at 0 deg	1.0	--
W2	"Second Order"	1.2	ω = .85 rad/sec ζ = .7
W1	"First Order"	1.0	1.0 rad/sec
W1, A	"First Order, Attenuated"	0.7	.40 rad/sec
A	"Attenuated"	0.53	--
ST	"Static"	0	--

Apparatus

The experiment was performed on the Dynamic Environmental Simulator (DES) at the Air Force Aerospace Medical Research Laboratory. The DES is a man-rated centrifuge with independent roll and pitch cab control. For this experiment only the roll tracking motion was used, with the roll rate limited to 90 deg/sec and the roll acceleration limited to 90 deg/sec^2. There are no limits on roll angle in the DES.

Within the cab the subject seat was mounted such that the roll axis of rotation was roughly through the subject's head. Mounted on the seat was a right-side-mounted force stick for vehicle control. The elbow was braced so that when the roll axis was 90 deg nose up, the hand was still comfortably over the stick. The cab contained a computer-generated display, Figure 2, which was centered in azimuth a distance of approximately 17 in. from the subject's eyes. The display was located such that it was within 0 to 10 deg of eye level for all subjects. The "inside out" display of target tracking error consisted of a 3.5-in. long rotating "target wing" whose center was superimposed upon a stationary horizontal dashed line 9 in. in length. A 0.25-in. perpendicular "fin" at the center of the rotating line provided upright orientation of the target.

The DES is configured such that the pitch gimbal is outside of the roll gimbal. Thus it is possible to pitch the simulator nose up 90 deg

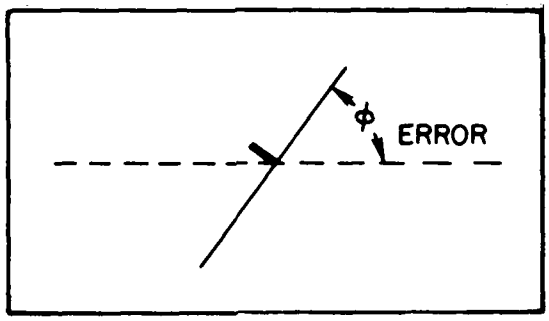

Figure 2. Sketch of the Roll Tracking Display

without affecting the roll axis tracking system. The cab pitched up 90 deg was used for the "real world" condition, as noted earlier.

Subjects

Four paid, healthy college students between 18 and 25 years of age were used for Experiment I. None were experienced pilots, so extensive training was necessary.

Procedure

Training and Data Collection Sequences

Training was first accomplished for the Static and two Full-Motion conditions. Tracking under each condition was considered one run. Each run lasted 165 sec and the 3 conditions or runs were presented in a random order each day. At the end of each run, subjects were presented their mean-squared-error score for that run. Training continued for approximately three weeks, three to six runs per day, at which time error scores finally began to reach asymptotic levels. Once performance leveled off, four more runs per subject per condition were performed, and time history data were recorded for subsequent analysis. The large number of training trials required to reach asymptote by non-pilots provided an incentive to use trained pilots in Experiment II.

For the second part of the study in which washout filter effects were investigated the experimental design philosophy stated earlier was used, i.e., washout filter effects should be compared to the "real-world" motion cues as encountered in the full motion no-tilt-cue case (F90). Therefore, at the start of the evaluation of each washout filter, each subject first tracked in the F90 condition for 1 day. Following this each subject tracked normally (roll axis at 0 deg) with a given washout filter for 3 days, four runs per day. The last four runs for each subject with the washout filter were saved for data analysis. The procedure was followed for each washout filter investigated. As in the first part of the study, subjects were told their scores for motivational purposes.

Measurements

A comprehensive set of measurements was made in order to quantify all aspects of the pilot's performance, behavior, and effort:

- Performance measures. Overall statistics (mean, variance, rms) of all signals, with emphasis on: tracking error, stick force, and physical roll angle and rates.

- Pilot behavior measures. Describing functions are the primary indicators of pilot behavior. The fitted parameters are useful for encoding efficiently the data, but the actual plots are often most informative. We use the "opened-loop" describing functions, as they are the most useful and tie in with past experience on single-loop systems (as explained later herein).

- Subjective evaluations. Each subject was given a questionnaire about his tracking strategy, effects of motion cues, and differences due to washouts. Because these were not experienced pilots, no comparison to actual flight could be made; instead, subjects were asked to compare the motion cues with those of the F90 "real world" case.

Data Analysis

From the time-history data recorded at various points in the loop noted in Figure 1, root-mean-squared values and Fast Fourier Transforms (FFT) of each time signal were computed. From the FFT, power spectral densities and opened-loop describing functions were computed. The frequency response data reduction, based upon the sum of sine waves generation, was similar to that employed in a preceding study (Levison et al., 1976). The specific transfer functions are given later herein.

Comparisons among individual data showed excellent consistency, once sufficient training had occurred. Therefore, for each motion condition, the last four runs of all subjects were averaged (16 runs total) by AMRL to give means $\pm$ standard deviation values for model fitting by STI. It is these averaged data that are analyzed in the later section titled Results.

Multiloop Parameter Identification Procedure and Pilot Model

Multiloop Analysis

The measurement problems involved in the multiloop system of Figure 1a can be illustrated by examining the task error components resulting from target and disturbance inputs, shown in Figure 3.

First consider the static case, where the Motion Response is inoperative: $M(j\omega) = 0$. Then the task error vector (frequency response function) becomes that given by Eq. 4 in Fig. 3 (for convenience, we have dropped the argument $s = j\omega$ in each of the inputs and transfer functions; $E(j\omega) = E$, etc.).

Equation 4 has been written in the form of a conventional single-loop system, wherein the [ ] term is the closed-loop error-to-input describing function, so the product $V \cdot Y_c$ is recognized as the open-loop describing function G_{OL} for purely visual feedbacks. Recall that increasing the magnitude of G_{OL} reduces tracking errors, etc. (e.g., see McRuer and Krendel, 1974).

Similarly, in hypothetical situations where the operator would close his eyes and operate solely on motion cues ($V = 0$), the task errors would be given by Eq. 5 in Fig. 3. The input is ignored, while the disturbances are suppressed.

When both visual and motion paths are active the multiloop relationships become more complex, but can still be written to reveal the effective "opened-loop" dynamics (similar to Eqs. 4 and 5), as shown in Eq. 6. Now, however, the opened-loop describing function for target errors (G_I, of Eq. 6a) contains the closed-motion loop $1/(1 + MWY_c)$, while G_D for the disturbance errors contain the sum of motion and visual effects $(V + MW)Y_c$.

In the single-loop cases of Eqs. 4 and 5 a high-gain (in V or M) reduces errors, but in the multiloop case there is a conflict:

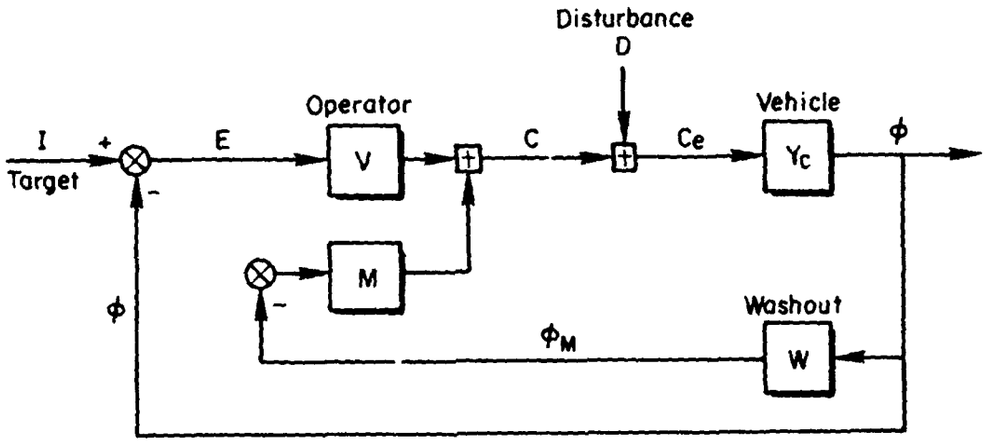

Note: All blocks and signals are vector functions of frequency: $E = E(j\omega)$ etc.

For Visual only: (Static; $M \equiv 0$)

$$E = (I - DY_c)\underbrace{\left[\frac{1}{1 + VY_c}\right]}_{(E/I)_{CL}} \tag{4}$$

Open-loop DF: "G_{OL}" for Visual Loop alone

For Motion Only: (Eyes closed; $V \equiv 0$)

$$E = I - DY_c\underbrace{\left[\frac{1}{1 + MWY_c}\right]}_{G_{OL}} \tag{5}$$

Open-loop DF: G_{OL} for Motion Loop alone

For Visual-Plus-Motion:

$$E = I\left[\frac{1}{1 + G_I}\right] + (-DY_c)\left[\frac{1}{1 + G_D}\right] \tag{6a}$$

where "Opened-loop" DF's

$$G_I = \frac{VY_c}{1 + MWY_c} \tag{6b}$$

$$G_D = (V + MW)Y_c \tag{6c}$$

Figure 3. Closed-loop Error Relationships to Target and Disturbance Inputs for Various Single and Multiloop Structures

- A high-gain motion feedback (large M) reduces the disturbance errors via Eqs. 6a and 6c, but increases the target errors via 6a and 6b.

- A high-gain visual loop (large V) reduces both error components.

- The optimum strategy (to minimize E) is a complicated function of the spectra of I and $D \cdot Y_c$, as well as of Y_c and W.

These are the analytical expressions for the qualitative motion/visual cue conflict mentioned in the Objectives section. Further, notice from Eqs. 6a and 6c that analytically opening the loop for either target or disturbance inputs will give different apparent opened-loop describing functions (G_I vs. G_D), even with identical V and M operations in both equations. This has led in the past to some misinterpretation of results for mostly target or mostly disturbance inputs.

Finally, it can be seen that, knowing the vehicle and washout dynamics (Y_c and W) and, given simultaneous independent inputs I and D, the independent estimates of the visual and motion operations (V and M) are theoretically computable if the signals are not confounded with noise. The temptation to measure V and M from static and motion-only runs, respectively, is precluded by the adaptive nature of the human operator. In general, the pilot will adopt different parameter values for his gains, leads and lags in the above special cases compared to the combined case, as will be shown later.

Pilot Model Structure and Parameters

The criteria for selecting the model structure are that it be:

a) The simplest form capable of capturing all of the significant frequency-domain characteristics of the measured data, both with and without motion.

b) Have components functionally related to previously well known visual-motor elements, such as neuromuscular (NM) and central nervous system (CNS) components, as well as motion sensing elements from afferent vestibular and proprioceptive signals.

c) Compatible with prior manual control models, e.g., those in McRuer and Krendel (1974).

Figure 4 details the assumed pilot model structure and forms for the Visual and Motion paths of Fig. 3. The rate and displacement elements in the "VISUAL PROCESSES" group are used to generate a lead time constant ($T_L = K_R/K_D$) which pilots typically adopt to cancel the roll-subsidence mode in the controlled element (Levison et al., 1976). The "integral" term is sometimes needed to represent the pilot's trimming actions and other low-frequency behavior (e.g., the so-called "α-effects" in the Extended Crossover Model of McRuer and Krendel, 1974). The extra visual time delays τ_V account for retinal and central (e.g., rate) processing as well as computational and display lags.

The tilt, velocity and acceleration terms in the "MOTION PROCESSES" are the simplest possible descriptors of the pilot's use of physical bank angle. These are not intended to represent motion sensors directly, although the velocity term is very similar to the output of the

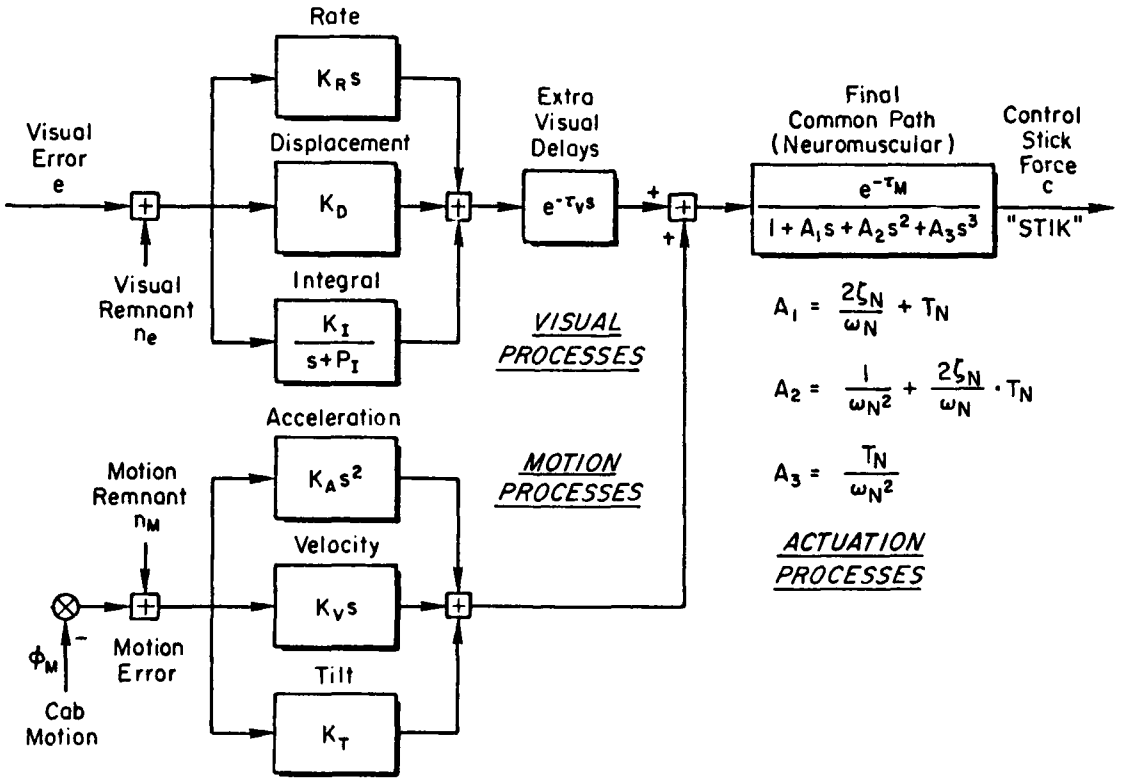

Figure 4. Assumed Pilot Model for Roll-Only Tracking

semicircular canals over the forcing function frequency region. The tilt angle cue K_T is actually due to the sensed lateral specific force due to the tilted g-vector.

The "ACTUATION PROCESSES" include a time delay τ_M and a third-order neuromuscular system, the latter readily simplified to a second- or even a first-order approximation, as noted in the figure (e.g., for a second-order system set $T_N = 0$, whence $A_3 = 0$, $A_2 = \omega_N^2$ and $A_1 = 2\zeta_N/\omega_N$). The delay terms τ_V and τ_M were actually modeled as first-order Pade polynomials,* and by breaking up the net delays into two small portions the Padé roots (at $2/\tau$) are at sufficiently high frequency to give an excellent fit up to over 10 rad/sec.

Identification

The two opened-loop expressions in Eq. 6a can be used to identify the two unknown paths (Visual and Motion) only if the Target and Disturbance inputs are independent. For signals constructed as a sum of sine waves this means that there can be no common frequencies. However this precludes the direct solution for the unknowns (V and M) since the opened-loop expressions cannot be evaluated at the same frequencies. This dilemma was dealt with in the earlier works (Shirley, 1968; Stapleford et al., 1969) by linearly interpolating the measurements at the interleaved frequencies. This can lead to difficulties and inaccuracies in the vicinity of lightly damped modes, where the transfer functions are not smooth. A different technique is used here, where specific model equation forms are assumed for the Visual and Motion paths and the equations of motion are written for all elements and loops, so that in effect the "interpolations" are made with appropriately shaped math models. The unknown parameters are then adjusted by the STI Model Fitting Program (MFP, described below) to fit simultaneously the

---

* $$e^{-\tau s} \doteq \frac{-(\tau/2)s + 1}{(\tau/2)s + 1} \quad ; \quad s < 2/\tau$$

closed-loop error and stick describing function responses to the Target and Disturbance inputs.

The STI Model Fitting Program was developed to fit high-order multi-loop models to frequency domain data (e.g., from Fast Fourier Transforms) and is described in Magdaleno and Allen (1975). It evaluates selected transfer functions from fixed-form adjustable-parameter equations of motion written in a special way, such that each adjustable parameter appears only once in the "matrix of equations." Thus, the influence of each parameter on any system response to any input is available. The program minimizes the vector difference between model and data transfer function responses using a variety of steepest descent techniques to minimize a cost function. This cost function is evaluated by summing the amplitude weighted squared differences in the real and imaginary parts of the describing function data and model responses at several frequencies. In the present case, five frequencies of the task error-to-disturbance, four of the stick-to-disturbance, and five of a linear sum of error- and stick-to-target were fit. The amplitude weighting was the inverse of the data magnitude, thus each frequency was uniformly represented except that the highest frequency of the stick-to-disturbance was weighted 10 dB less.

Since the target and disturbance are sums of sinusoids, the effective opened-loop expressions in Eq. 6 were estimated using ratios of Fourier coefficients:

$$\hat{G}_I(j\omega)\Big|_I = \frac{\phi}{E} = \frac{PLNT}{VERR} \qquad \text{at Target frequencies, } \omega_I \tag{7}$$

$$\hat{G}_D(j\omega)\Big|_D = \frac{-C}{C_e} = \frac{-STIK}{SERR} \qquad \text{at Disturbance frequencies, } \omega_D \tag{8}$$

where the four character names PLNT, VERR, STIK, and SERR are defined in Figure 1 and will be used to identify various responses in the remainder of this report.

To check the accuracy of this procedure an analog "autopilot" operation on both task error and measured motion was mechanized on the DES setup and the recorded signals were processed through MFP. Table 3 summarizes the results of this calibration, using the forms indicated. The time delay shown is an approximation to the net phase effects of various hybrid computation delays and high-frequency anti-aliasing filter lags. Some errors could be due to the fact that the "dialed in" computer settings did not accurately represent the effective parameters. Generally the recovered parameters in Table 3 are quite close to the simulated values, such that a transfer function plotted from the recovered parameters would be indistinguishable from one plotted for the simulated parameters.

TABLE 3

SIMULATED AND RECOVERED PARAMETERS FOR DUAL INPUT AUTOPILOT

$$\text{Visual Path:} \quad V = \frac{K_R s + K_D}{T_V s + 1} e^{-\tau_V s}$$

$$\text{Motion Path:} \quad IM = \frac{K_V s + K_T}{T_M s + 1}$$

CASE	"VISUAL LOOP"				"MOTION LOOP"		
	K_D	K_R	T_V	τ_V	K_T	K_V	T_M
Simulated	.133	.067	.100	.018	.040	.100	.100
Recovered by MFP	.134	.062	.098	.023	.040	.104	.092

RESULTS AND DISCUSSION

Presentation Format

The presentation of all the reduced and averaged data is not needed. Instead, we present typical time histories for one subject, then spectra and describing functions averaged over four subjects (4 runs each) for a typical motion case. Finally, after demonstrating that the fitted transfer functions truly represent the data, we present the averaged fitted data and curves for each of the cases and analyze the resulting performance and behavioral measures to answer the objectives stated in the Introduction.

Typical Time History

A matched pair of time histories of the various inputs and outputs for corresponding segments of static and full-motion runs is given in Figure 5. For these runs, identical target and disturbance inputs (top and bottom traces) were used to reveal the static-motion differences more clearly.* The following features of the time histories should be noted:

- Ideally, the A/C Roll Angle, (ϕ, second line) should match the target roll angle, (ϕ_i, top line).
- Although not shown separately the disturbance input, d, which is summed just downstream of the pilot's control force, c (and shown to the same scale), is effectively integrated by the vehicle dynamics to yield roll error motions comparable in amplitude and frequency to the target input.
- In the static case the roll angle does not follow the target very well, because of these simultaneous, large roll disturbance effects.

*Normally the initial phases of the sinusoids in each input were randomized to prevent repetition of, and thus learning of, the input patterns. This set of runs with identical inputs was made especially for this report.

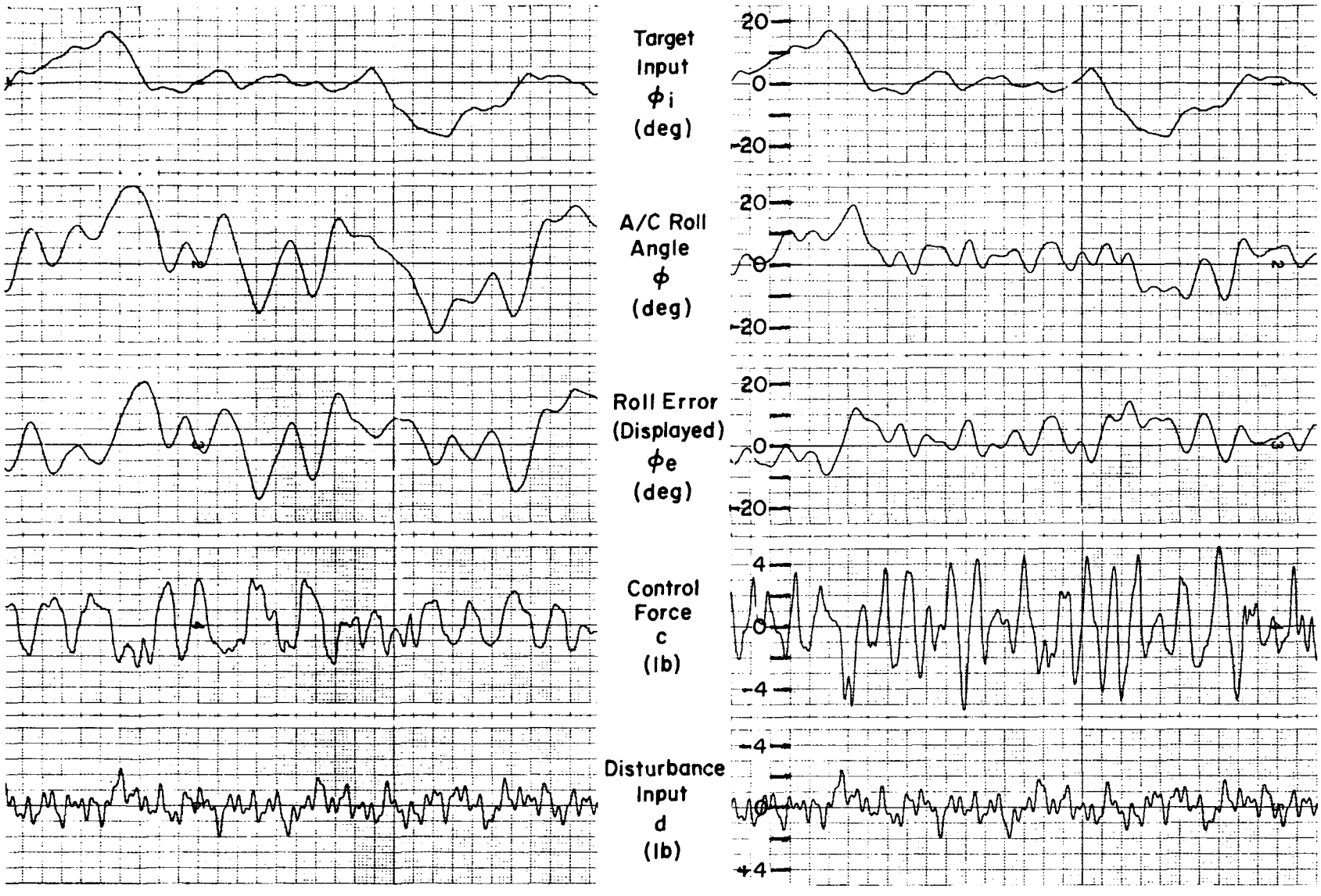

Figure 5. Typical Time Histories with No- and Full-Motion

- Comparison of the ϕ_e and c traces for the static case, where only the visually displayed error can be used, shows that the pilot is using both error displacement and rate in his compensating control actions. (The c peaks are roughly opposite to, and slightly lead, the ϕ_e peaks.)

- Comparing the motion case to the static case, the control response, c, is obviously more aggressive and has higher bandwidth (due to motion cues), while the tracking error is reduced. Whereas ϕ overshoots ϕ_i for the static case, it often undershoots for the motion case.

- There is a remarkable consistency (not shown here) in the ϕ, ϕ_e, and c traces for repeated portions of the same inputs, showing a highly input-coherent and consistent operator response, as will be shown later by the reduced data.

Frequency-Domain Data and Model Fitting

Examination of the individual error scores and closed-loop describing functions showed that each of the subjects adopted similar behavior. Thus, the results could be validly averaged, without loss of significant details in the average. Approximately four runs per condition for each of the four subjects were averaged for the data shown. (The data shown here for the Full Motion Case with roll axis at 0 deg are genuinely typical of all the cases investigated and were not selected as the best available example.)

Spectra

Figure 6 shows power spectra for the control stick, displayed error, and aircraft bank angle. The "remnant" (plotted at forcing function frequencies by the ✖ symbols) is actually an average of the non-coherent power over neighboring (nonoverlapping) estimates. The small standard deviations shown for all signal components indicate that all subjects had essentially the same, low variability, behavior. The signal-to-noise ratio is quite good (15-20 dB or 5-10:1) at all but the very highest frequencies and implies a high coherency between the two

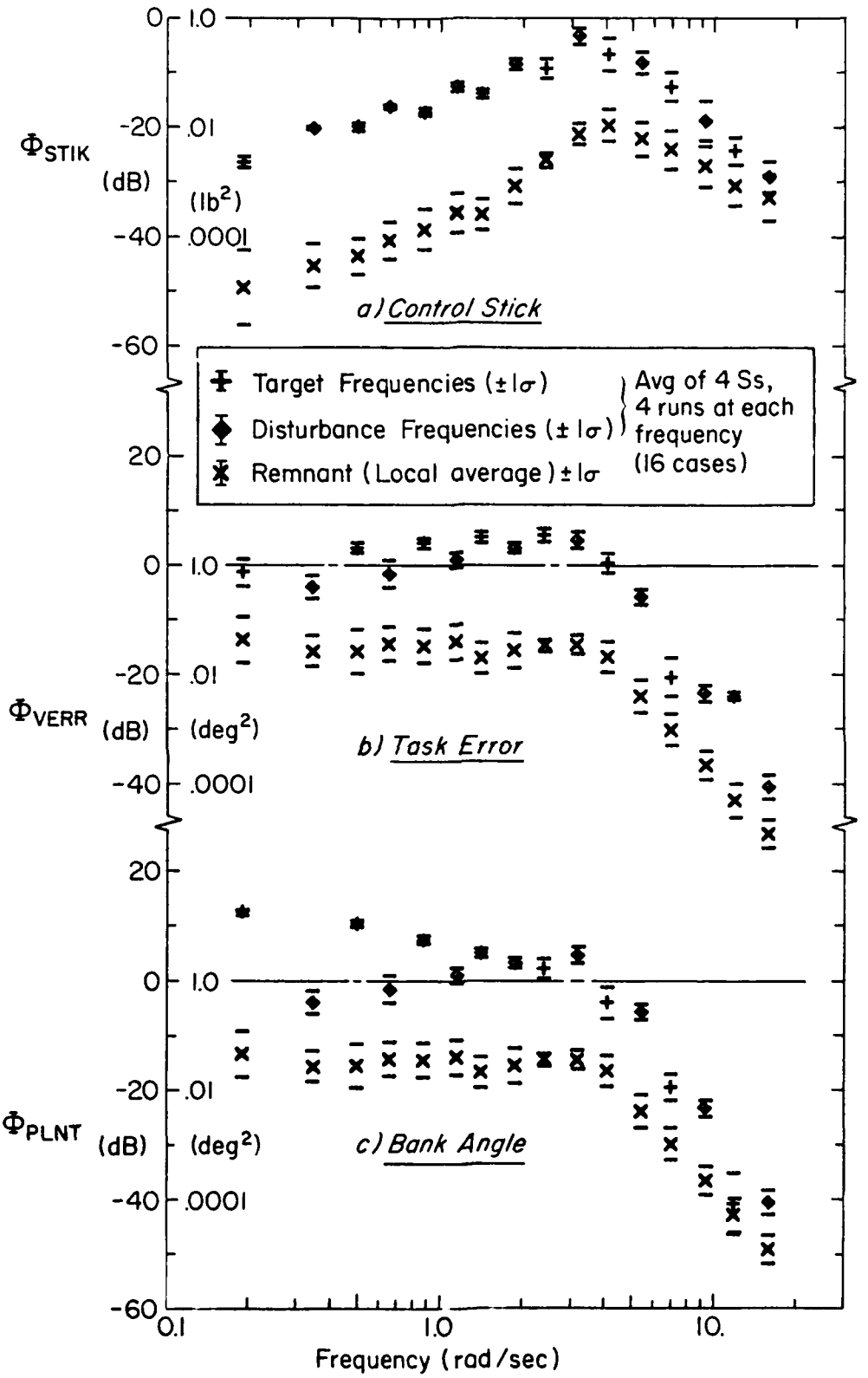

Figure 6. Typical Power Spectra for Full Motion, Erect (Case F0)

inputs and responses. This permits the major part of the responses to be described by linearized describing functions. Notice that the spectrum of Φ_{plant} (+ symbols) in Figure 6c is large at the lowest target frequencies (to follow the target), while its spectrum at the lowest disturbance frequencies (◇) is lower, as desired. The pilot is clearly following the target inputs and suppressing the disturbances below about 1 rad/sec.

Closed-Loop Describing Functions

Figure 7 illustrates typical closed-loop describing function data (to which the model was fitted by the MFP procedure described earlier) for the control stick and task error responses to target and disturbance inputs. The frequencies used in the model fits are indicated by the arrows labled "Fitted Freqs." Not all data points were used for computational economy. A preliminary analysis indicated that the 19 selected frequency response points were the most sensitive indicators of pilot behavior.

Generally, the closed-loop data exhibit very low variability and the model fits (solid lines) capture every nuance of all the responses, using one set of model parameters and the various closed-loop relationships (e.g., from Figure 3). The peaks and dips in the describing functions due to various low-damped modes would greatly complicate simple interpolations between target frequencies to obtain vectors at disturbance frequencies, as done by earlier investigators.

Model Fits

Table 4 summarizes the model parameters fit to the data for all dual-input cases. Only nine of the twelve parameters in Figure 4 were needed, as preliminary fits showed that a second-order fit was sufficient for the neuromuscular mode ($T_N = 0$) and there appeared to be no error integrating action ($K_I = P_I = 0$). Lack of K_I and P_I (the so-called α-effect in the Extended Crossover Model) may have been due to the presence of the tilt cue in the motion cases with roll axis at 0 deg, but its absence at F90 and Static conditions is unusual.

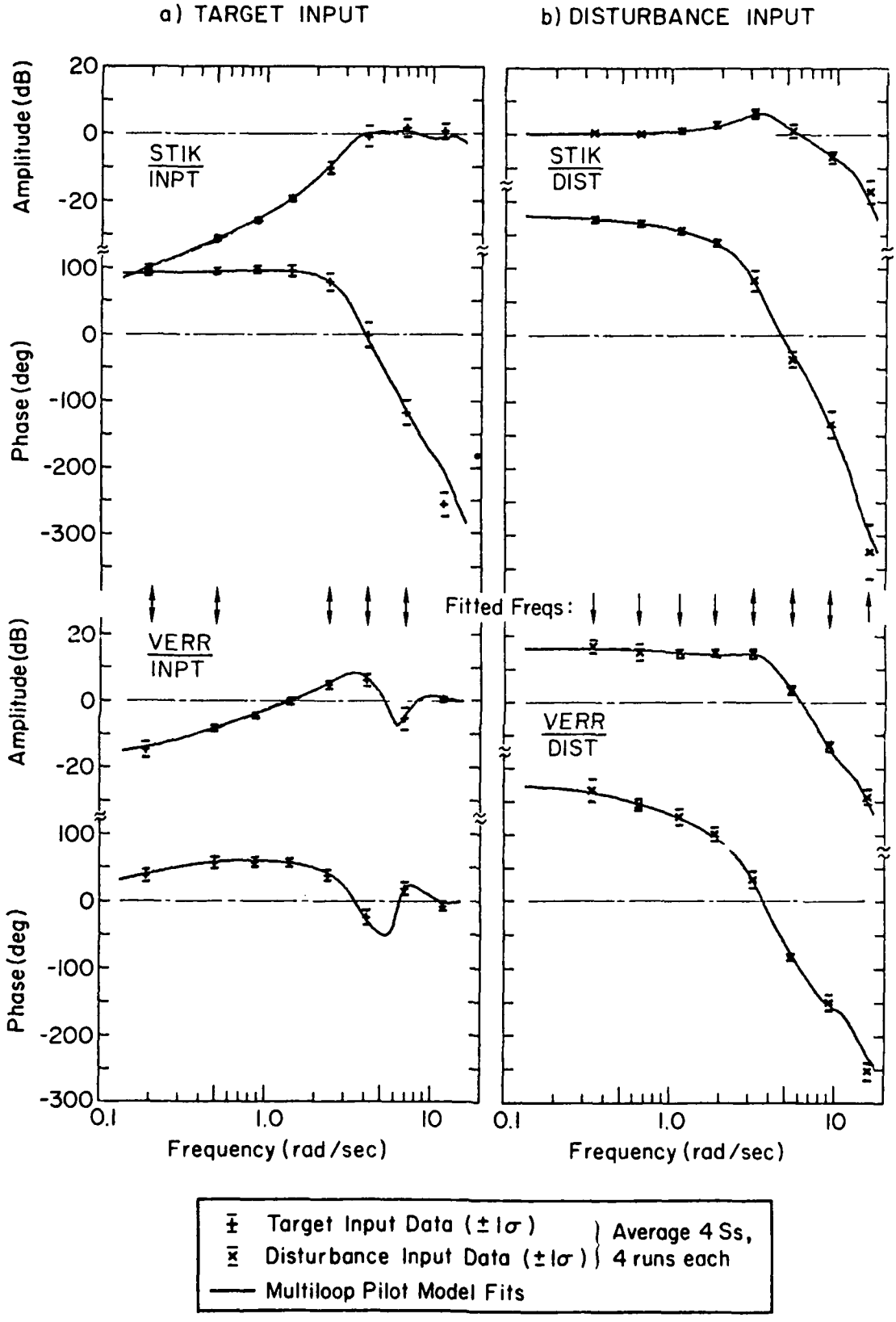

Figure 7. Typical Closed-Loop Describing Function Data and Model Fits for Full Motion, Erect (Dual Input, Case F0)

TABLE 4. SUMMARY OF PILOT MODEL PARAMETERS FIT TO DATA

CASE Motion Condition	MODEL PARAMETERS												REMARKS
	Visual					Motion			Neuromuscular				
	K_D	K_R	τ_V	$T_L = \frac{K_R}{K_D}$	$\frac{K_R}{K_D} - \tau_V$	K_T	K_V	K_A	τ_M	ζ_N	ω_N	$\tau_M + A_1$	
	$\frac{lb}{deg}$	$\frac{lb}{deg/s}$	sec	sec	sec	$\frac{lb}{deg}$	$\frac{lb}{deg/s}$	$\frac{lb}{deg/s^2}$	sec	—	$\frac{rad}{sec}$	sec	
F90 Real World	0.149	0.068	0.16	0.46	0.30	-.0001	0.076	0.020	0.15	0.26	9.3	0.20	Theor. $K_T \approx 0$
F0 Full Motion	0.136	0.074	0.15	0.54	0.39	0.022	0.070	0.022	0.15	0.29	10.4	0.20	$\tau_M + A_1$ = Effective NM Delay
W2 2nd Washout	0.134	0.090	0.12	0.67	0.55	0.023	0.048	0.019	0.11	0.39	7.6	0.22	
W1 1st Washout	0.130	0.079	0.12	0.61	0.49	0.034	0.060	0.022	0.11	0.38	7.6	0.21	
W1, A 1st Wash + Atten.	0.119	0.070	0.08	0.59	0.51	0.040	0.081	0.031	0.17	0.28	9.0	0.23	
A Atten. Motion	0.122	0.053	0.06	0.43	0.37	0.056	0.131	0.028	0.15	0.13	8.2	0.19	K_T, $K_V \approx$ twice Values for F0
ST Static	0.072	0.064	—	0.89	—	—	—	—	0.18	0.18	7.0	0.23	

(K_1, P_1, A_3 set to 0)

The additional columns in Table 4 detail the effective lead time constant in the visual path ($T_L = K_R/K_D$; $T_{L_{eff}} = [K_R/K_D]e^{-\tau V}$) and the effective time delay in the neuromuscular path ($\tau_e \triangleq \tau_M + A_1$). Note that the visual displacement gain, K_D, nearly doubles when going from Static to any Motion condition, and the tilt sensitivity, K_T, is negligible for the F90 case, as it should be, since no tilt cue is available.

Opened-Loop Describing Functions

A number of other trends and covariations among parameters are evident; however, these effects can best be illustrated by using the opened-loop responses calculated using the measured closed-loop data along with the loop structure of Figure 3 or the parameters in Table 4 with the model of Figures 3 and 4. Figure 8 shows the resulting opened-loop data and computed model curve for the Full Motion, FO, case. As with the closed-loop responses the model curve fits the actual opened-loop data very well — it truly represents the data. These data and fits for this example are typical, i.e., the other cases show effects similar in kind, differing only in degree. Thus, comparisons among cases can be made using the curve fits, as we will do in the remainder of this report.

These multiple opened-loop describing functions have all of the appearance and significance of single-open-loop transfer functions, and similar descriptive parameters apply. Some of these have been noted in Figure 8, as defined below:

ω_u = "Unstable frequency" (180 deg phase crossover). This sets the maximum bandwidth of the loop, and is the frequency at which oscillations would set in if the gain were further increased by K_M dB.

ω_c = "Crossover frequency" (0 dB gain crossover). This sets the effective bandwidth of the loop, and determines the resulting stability margins.

K_M = "Gain margin" (dB). Allowable gain increase for incipient loop instability.

ϕ_M = "Phase margin" (deg). Allowable phase lag increase for incipient loop instability.

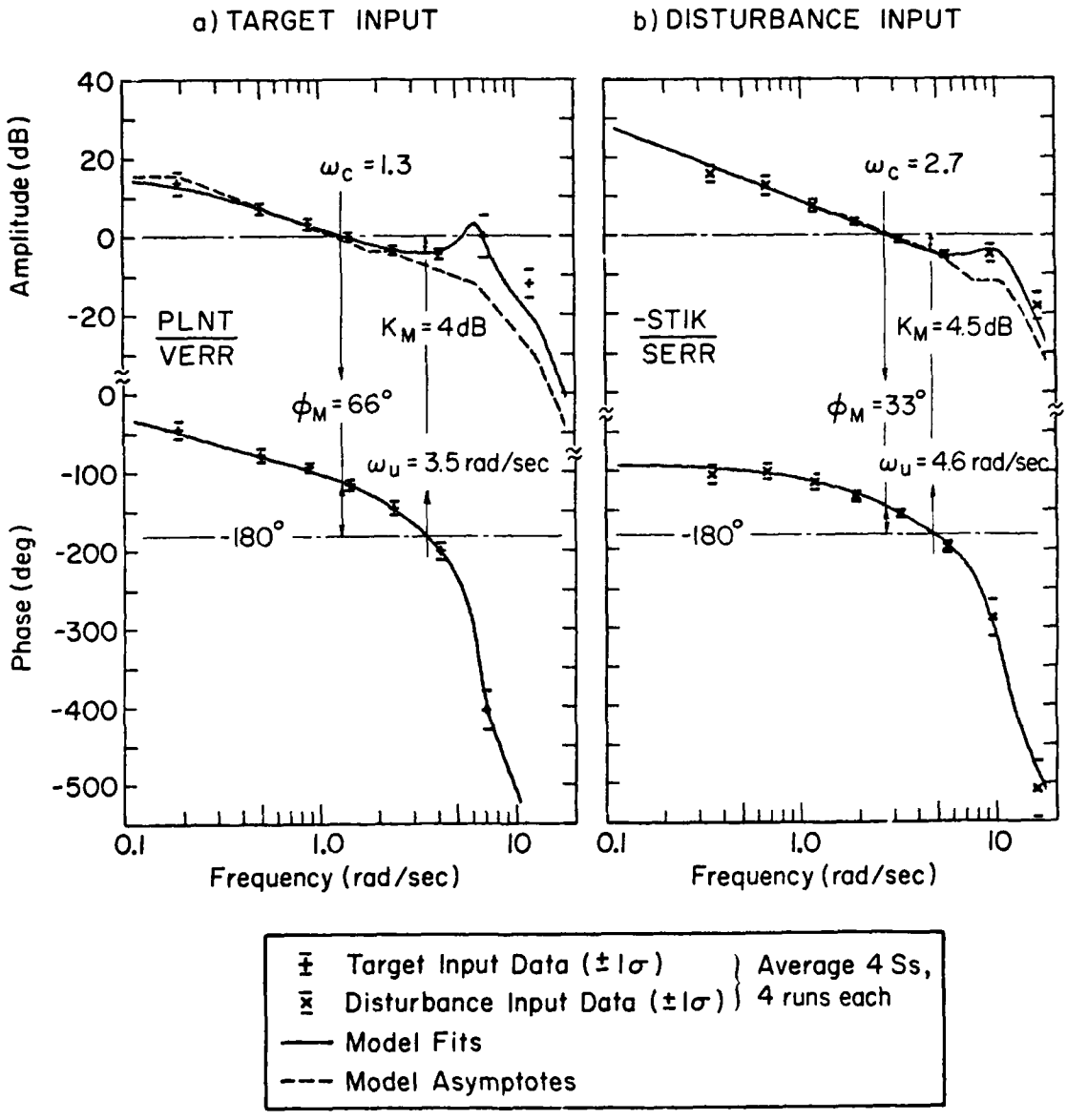

Figure 8. Typical Effective "Opened Loop" Data and Model Curve for Full Motion, Erect (Dual Input, Case F0)

In Figure 8 it is apparent that the disturbance loop (dominated by the motion pathway) has a higher bandwidth and a lower phase margin than the target loop (dominated by the visual pathway). This implies lower tracking errors, as will be shown later.

The kinks in the dashed "asymptotes" in Figure 8 show the poles (break downward) and zeros (break upward) of the model. The need for the relatively high-order pilot/vehicle model used here is shown by the spread between the asymptote breaks and the model fits, as well as the different asymptotes in each opened loop. As in the closed-loop cases of Figure 7, the precise fit of the opened-loop model in Figure 8 captures every nuance of the raw data.

Effects of Full Motion vs. Static Conditions

Figure 9 compares various performance measures for Full Motion and Static cases. Variances are used because they can be partitioned into additive vector components due to: Target, Disturbance, and Remnant. (The right-hand scale of each variance plot is scaled to the corresponding rms levels, and the forcing function levels of target and disturbance are shown by arrows.) Concentrating on task error, Figure 9b, for the Static case, the error components from Disturbance (D) and Target (T) inputs are essentially the same, reflecting the dual input spectrum design objective mentioned earlier. For the Full Motion, Supine case (F90) the target errors are the same as for a Static cab, while the disturbance errors are much smaller. Going from Full Motion, Supine to the Erect case (F0) shows that the target-following errors are reduced slightly while the disturbance errors are unchanged. The roll angle data in Figure 9a show that for the "real world" F90 and Static cases the Target-related angles (T) quite closely matched the input, σ_{ϕ_T}, while this component was reduced in the erect (F0) case.

These basic trends in the tracking performance are explained by the changes in the opened-loop describing functions (DF) shown in Figure 10. For the Target Input DFs the Supine and Static cases, each having no tilt cues, show essentially the same DF (which results in the same target-following errors), whereas the Erect case (with the maximum tilt

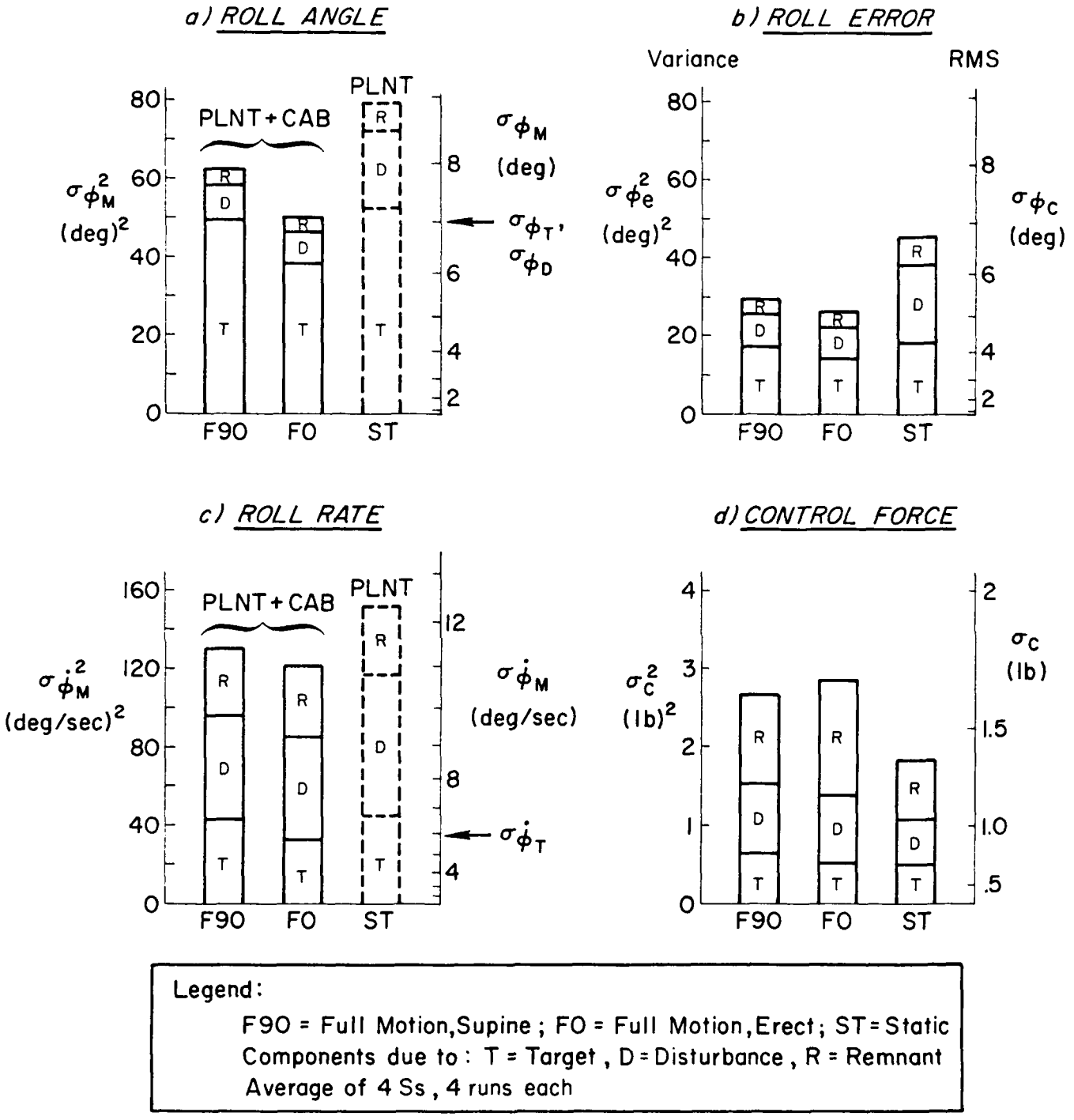

Figure 9. Effects of Full Motion (Supine, Erect) and Static Cases on Performance

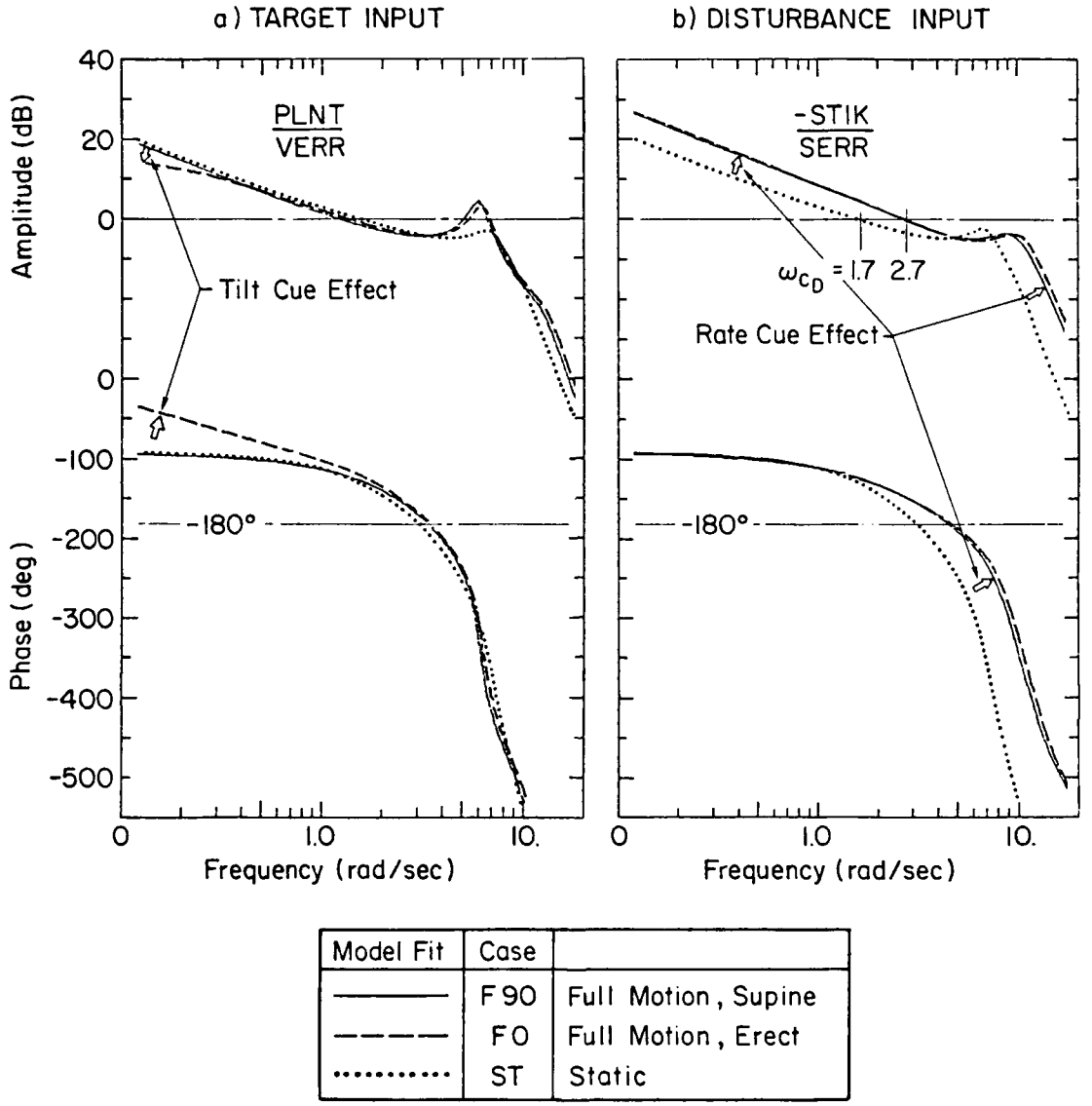

Model Fit	Case	
———	F 90	Full Motion, Supine
– – – –	F 0	Full Motion, Erect
.....	ST	Static

Figure 10. Effect of Motion Cues on "Opened Loop" Describing Functions (Dual Input Cases)

cue) has a smaller target error. For the Disturbance Input, both motion cases (F0, F90) have the same DF, which explains why their "D" components were the same in Figures 9a, b, c, d. Furthermore, the "Rate Cue Effect" (lower loop lags leading to higher crossover frequencies with motion) leads to the motion/static performance effects denoted by the arrows in Figure 10. Thus Figures 9 and 10 show that the subjects used motion cues to improve performance in two main ways:

- The lower lags (and higher crossover frequencies) permitted by the vestibular sensory-motor loop enable, in effect, a "roll-rate damper loop" to be closed by the pilot, thereby allowing a tighter disturbance regulation loop to be used by him (a loop gain increase of about 2.7/1.7 = 1.6). Consequently, the disturbance variance is reduced significantly.

- The tilt-cue was used at low frequencies to provide a sense of zero reference and, thereby, to avoid drifts and overshoots, the effects showing up as a low-frequency phase reduction on the target "opened loop."

Components of the Multiloop Describing Function Under Motion

Further insight may be gained into the complexity of the multiloop interactions and motion effects via Figure 11, in which the fitted model has been used, via the loop structure and equations of Figure 3, to examine: each sensory loop individually (visual = dashed, motion = dotted) with the other simply turned off, and then the combined opened loop (solid line) as discussed earlier. Remember that the opened-loop DF is a complex vector function of V and M, as noted in the legend.

The key points revealed by Figure 11 are as follows:

- The Disturbance Input loop (on the right) is a simple vector sum of VY_c and MY_c. The flat amplitude of the motion loop (dotted) shows that MY_c acts like a roll-rate feedback loop with an effective time delay, τ_e, appreciably less than the visual loop (for MY_c, $\tau_e \triangleq 0.20$ sec; for VY_c, $\tau_e \triangleq 0.20 + 0.15 = 0.35$ sec). Over the important crossover frequency region of 0.5-5.0 rad/sec, their vector sum (solid) has an apparent τ_e even <u>less</u> than MY_c alone! This is consistent with, and "explains," the results of Stapleford et al. (1969) and Shirley (1968), i.e., the combined case, with motion, acts as if it were

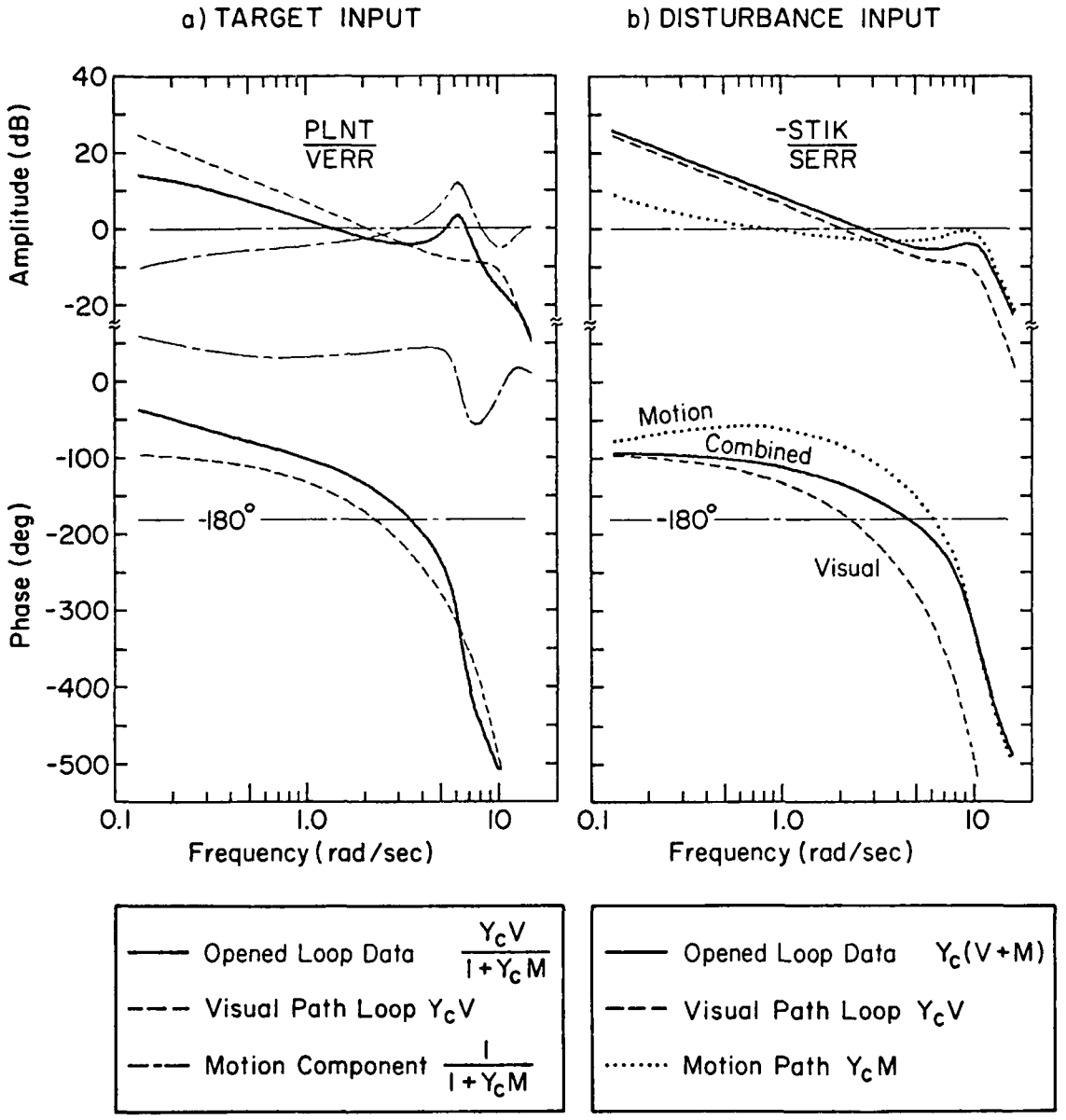

Figure 11. Behavioral Components of "Opened Loop" Data (Dual Input, Full Motion, Erect Case F0)

like a visual-only loop in amplitude but has a lower phase lag like a lower τ_e.

- Disturbance regulation (solid) is dominated by (closest to) the visual loop at low frequencies and motion loop at high frequencies.

- The Target-following loop (on the left) is a more complex function of VY_c and MY_c as seen in the equations shown in the box. (The motion component $(1 + Y_cM)^{-1}$ is shown dash-dotted to distinguish it from Y_cM alone. Here, the solid curve is the vector product of the two components.) In both amplitude and phase, the Target-following loop dynamics are dominated by the visual loop (dashed) at all frequencies.

- A comparison (not shown here) of the purely visual static case per se (dotted curve of previous Figure 10) and the isolated VY_c (dashed curve of Figure 11) shows that they are not the same. When motion is present, the visual loop can be (and is) operated at higher gains, albeit with a slightly larger lead equalization (T_L) and consequently larger τ_e. (Per Table 4, $T_L \triangleq 0.89$ sec and $\tau_e \triangleq 0.23$ sec for the ST case; while $T_L = 0.54$ sec and $\tau_e = 0.20 + 0.15 = 0.35$ sec for the FO case.)

This analysis of Figure 11, and others like it, clearly shows that one cannot simply add a motion feedback loop to the static case dynamics to get the combined result. Instead, the operator optimizes his combined loop properties for the case at hand.

Effects of Single vs. Dual Forcing Functions

For two Full Motion cases (F90, FO), data were taken for Target input alone; and for Case F90, Disturbance input alone, to compare with the dual input case. When either input was used alone, it was increased by 2-1/2 to keep the rms input the same as in the dual input case.

In general one might expect that if the disturbance alone were present, the pilot would adopt a different optimum behavior, because all he would have to do is to suppress both the felt and seen motions. Conversely, for the target alone, the pilot might more aggressively track the error, because the unseen disturbances were absent.

The results, shown in the opened-loop describing functions in Figure 12, did not follow these expectations! For simplicity, the curve in Figure 12 is that fitted to the corresponding dual input case, for which it passed precisely through every data point on both sets of DF (e.g., see Figure 8). The single-input data are shown relative to this dual-input curve in Figure 12, remembering that each of the data plots represents a different set of runs. Somewhat to our surprise, the single input data are not significantly different from the dual input case, for the points generally lie within one symbol width of the curve and almost all lie well within ±1 standard deviation of the dual-input curve.

How can this be, in the light of the theoretical expectations discussed above, considering that all pilots were given extensive practice on every case and noting that all behaved similarly (evidenced by the low scatter)?

Some hypotheses are

- There was some error in the experiment, such that dual inputs were really present. We checked this and verified that only the specified single input spectra and rms signals were present.

- The "optimum" behavior was, perhaps fortuitously, nearly identical for the single and dual input cases. The combination of lightly damped modes in the controlled element near the neuromuscular modes plus stick lags has been identified as the so-called "Pilot Induced Oscillation Syndrome" of Ashkenas et al. (1964). These restrict the degree of equalization which can be used by the pilot to improve performance. Consequently, he may be operating near this constrained limit in all cases.

- The pilots were so overtrained in the dual case that they did not adopt "optimum" behavior in the single input cases despite extensive practice with it. If so, this raises questions with respect to the assumption that pilots adopt an "optimum" behavior for the case at hand.

This would be an ideal, simple test case against which to validate the optimal control models (e.g., Levison and Junker, 1977). The inputs are analytically tractable, the good model fits show that the data are representable by linear, modest-order state equations; and the data are precise, have high signal-to-noise, and are internally self consistent.

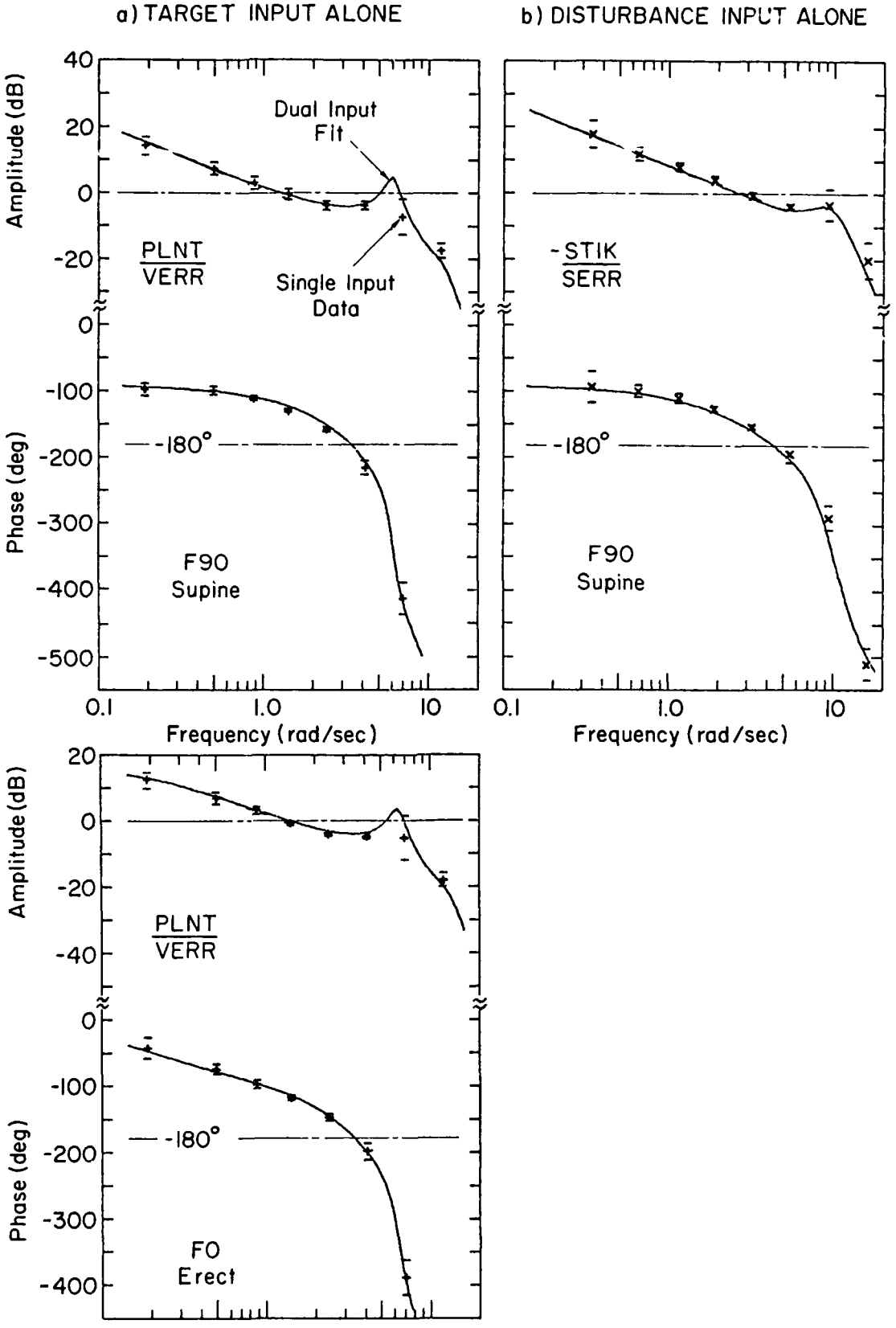

Figure 12. Comparison of Single Input Data with Model Fit from Dual Input Data

Such a validation remains as a challenge for the optimal control model practitioners!

Meanwhile, this result tentatively implies that the dual-input results should apply to the single input situations, if the inputs and controlled elements are similar to those used herein.

Effects of Motion Shaping (Washouts)

Having presented the results on our first question — that of basic motion effects versus no motion — we turn now to the second question: what are the effects of various motion "shaping" (attenuations and/or washouts)? For this purpose, the data will be restricted to the dual-input cases, all with roll axis horizontal, i.e., FO, W2, W1, W1A, ATT, in the order of decreasing recovered roll angle.

Figure 13 shows various performance measures for these cases. Consider first the variance of recovered (measured physical) roll angle, $\sigma^2_{\phi_M}$, shown at the upper left, with each case broken down in terms of the components due to target, disturbance, and remnant. Noted on the margin are the variances for the untracked target (or disturbance) input alone, and their sum. Ideally, the recovered variance would consist of only the target component (equal to $\sigma^2_{\phi_T}$, attenuated by the motion shaping washout) and no disturbance or remnant portions. It may be recalled from Figure 9 that in the "real world" (F90) case this ideal is approached, in that the target component nearly equals the commands while the disturbance and remnant portions were small fractions of that.

With these standards in mind, let us consider the effects of various washouts. As described in the section on Approach, the overall scheme was to select different forms of motion washout, each selected (albeit crudely) to attenuate roll angle to about 50 percent of the basic, FO, case (i.e., the target roll variance of 25 percent of the basic level). As seen in Figure 13a, this was achieved closely only for the pure attenuation case ($\sigma_{\phi_M} \triangleq 3.6$ deg versus $\sigma_{\phi_T} \triangleq 7.0$ deg). The ATT computed roll motions (shown dashed) were nearly equal to the FO case, as were the other task performance measures in Figure 13 (e.g., tracking

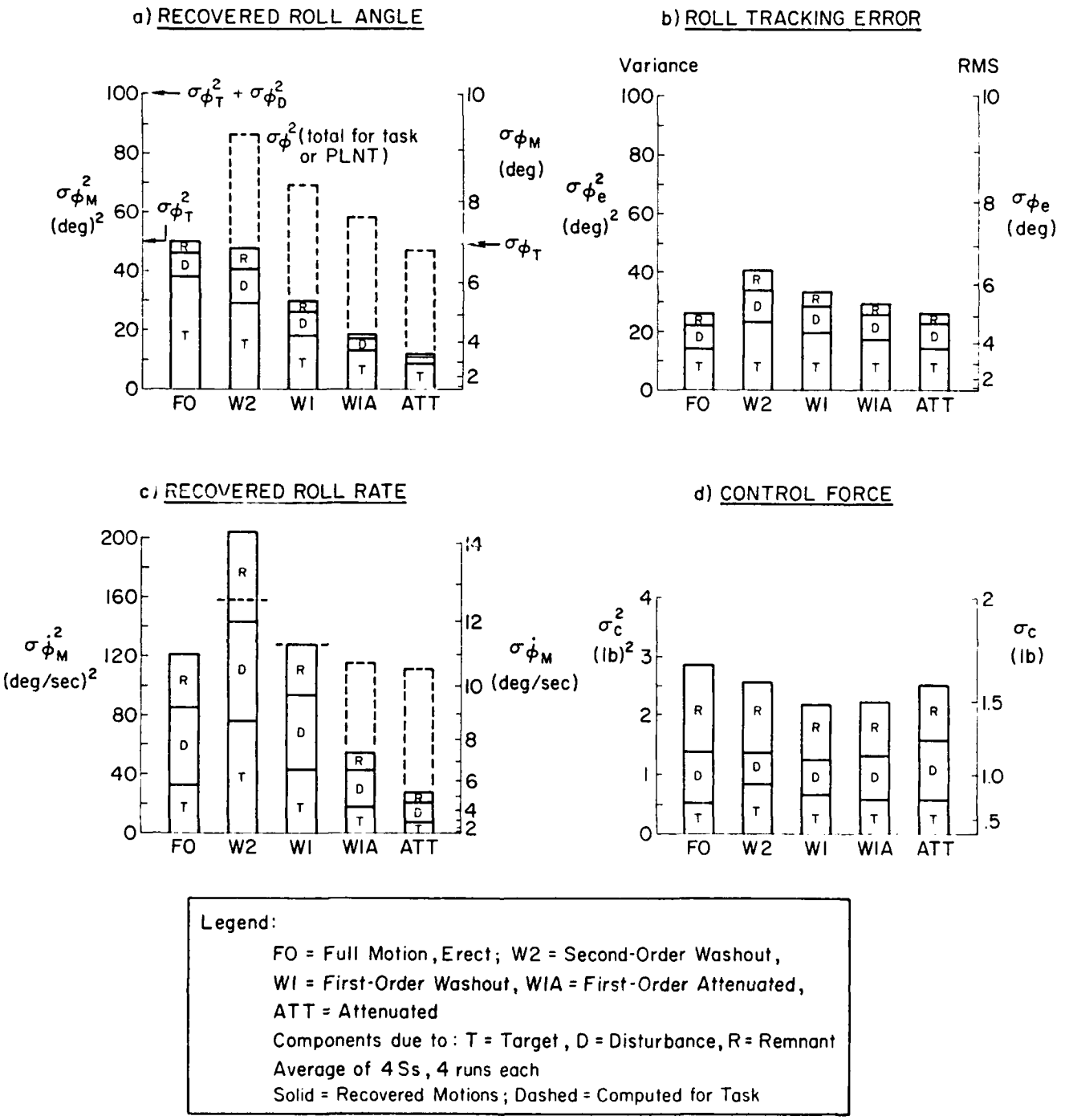

Figure 13. Effects of Motion Shaping on Performance

error and control force), implying a proportionate scaling of the visual and motion loop behavior in the FO and ATT cases despite the lower magnitude of motion cues in the latter. (This will be discussed later in greater detail.)

The second-order washout (W2), which greatly attenuates the lowest frequencies, distorted the perceived motion cues (per the subjective questionnaire) and failed to reduce the motions as intended. Analysis of these results showed that this was due to the following reasons:

a) The washout was a compromise design* such that the high-frequency asymptote magnified the roll angles (and rates) above the break frequency of 0.85 rad/sec by a factor of about 1.2, causing the roll rate variance (Figure 13c) and high-frequency portions of the roll angle variance to be increased by $(1.2)^2 \doteq 1.4$ relative to the intended case.

b) The phase distortion of the felt motions relative to the visual motions caused the pilots to perform even worse than in the static case.

The other washouts were intermediate in recovered motion and plant motion between the Full and Attenuated cases.

Attenuation reduces both the recovered roll <u>angles</u> and roll <u>rates</u> in the same proportion, but washout reduces mainly the low-frequency components and thereby reduces the roll rates less than the roll angles. This can be seen by comparing Figures 13a versus 13c, particularly for the W2 and W1 cases.

Except for the anomalous W2 case, discussed above, the performance measures of tracking error and control force were not significantly different among any of the first order or attenuated washout cases (see Figures 13b and 13d). Even the proportions of each variance due to

*The DES is a velocity command system and as such would drift whenever a cascade washout was used. Consequently, a feedback scheme was devised that approximated the desired cascade washout, but a perfect match at both high and low frequencies was not possible.

target inputs, disturbances, and remnant were about the same as for the full motion case (FO).

Further insight into the pilot's tracking behavior under these washouts is given by the opened-loop describing functions for the various cases in Figure 14. It is immediately apparent that the disturbance-loop describing functions are nearly identical, implying the following:

- Despite attenuated, reduced low-frequency motions, and phase distortions, the pilot compensated to give the same opened-loop DF.

- In the ATT case the rms roll angle was reduced from 7 deg to 3.6 deg, the pilot had to double his tilt and roll rate gains (K_T, K_V) as verified by the fitted coefficients in Table 4 and summarized below:

Case	σ_ϕ (deg)	K_T	K_V	K_A
Full Motion, FO	7.	0.022	0.070	0.022
Attenuated to 0.50, ATT	3.6	0.056	0.131	0.028
Ratio, ATT/FO	0.51	2.55	1.87	1.27

  Despite the fact that the rms tilt angle in the ATT case represents a lateral-specific-force cue of less than $3.6/57.3 = 0.063\ G_y$, the roll rates were apparently sufficiently high to be readily sensed and used to compensate for the reduced motion cue over the FO case.

On the left of Figure 14 is the target loop DF, where the following effects of washout are clearly apparent:

- The FO and ATT cases are nearly identical for the same reasons given above for the invariant disturbance loop DF.

- The washouts induce (at low frequencies) higher amplitude ratio and more phase lag as the washout order is increased from ATT to W2. An analysis indicates that these trends reflect fairly complex interactions similar to that shown earlier in Figure 11 (left side). Note that inserting a low-frequency washout to the motion path (M in Figure 11) causes the resulting curve to start (at low frequencies) on the dashed curve and transition to the solid curve with increasing frequency. Those amplitude and phase trends of

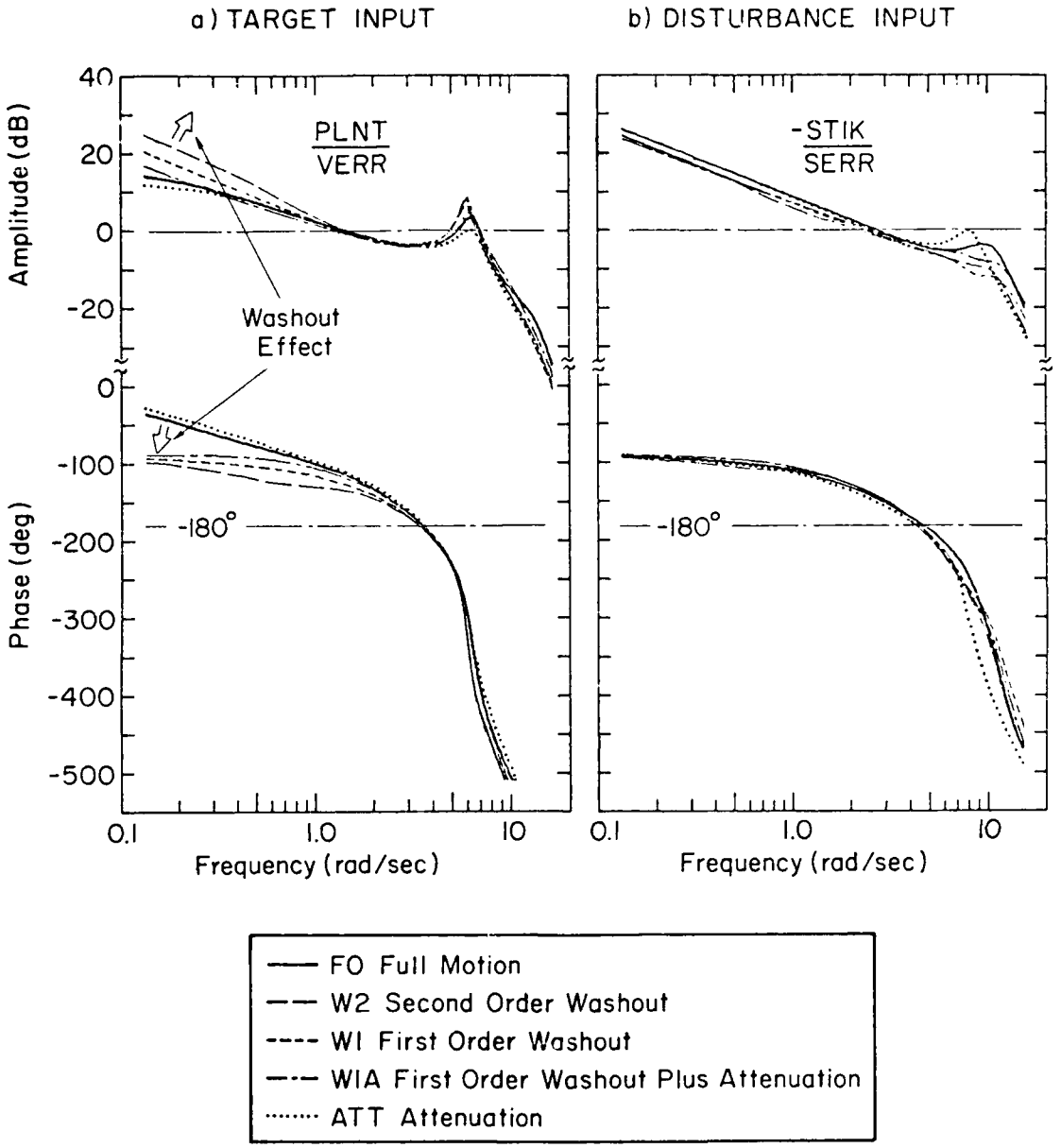

Figure 14. Effects of Motion Shaping for Opened Loop Describing Function (Dual Input Cases, Roll Axis Horizontal)

Figure 11 also explain the "Washout Effect" in Figure 14. It also appears that those washouts having highest phase distortion (pure first and second order, shown dashed in Figure 14) cause the pilot to depend more on visual information than motion at low frequencies.

Optimum Washout

One of the objectives of this experiment was to find the optimum washout for AMRL's roll-only simulators. Relative to the "real world" case, the desirable criteria are: a) a significant reduction in roll amplitude and rates; and b) similar pilot behavior and performance.

Inspection of the foregoing results reveals that the clear choice is the first-order attenuated washout (W1A). Figure 15 justifies this selection based on the following comparisons with the F90 ("real world" baseline) case:

- Large reduction in recovered roll angle and rate, as shown in Figure 15a, with similar plant roll angles and rates.
- Very similar tracking error performance and control activity, as shown in Figures 15b and 15c. Even the distributions of each variance from target, disturbance, and remnant inputs are closely matched.
- The opened-loop describing functions, shown in Figure 15d, are practically identical. This is because the effect of tilt cue usage previously described in connection with Figure 10, is almost exactly cancelled by the washout-break effect noted in Figure 14.
- (Not shown) The subjective comments were more favorable for this washout than for any other except pure attenuation.

Thus, we recommend first-order attenuated washout for use on all AMRL roll-only type simulators. The degree to which this form can be extended has not been determined, but the data suggest the following as likely to be both useful and satisfactory to pilots:

- Attenuation factor of 0.5 to 0.7.
- Break frequency of 0.3 to 0.5 rad/sec (washout time constant of 2-3 sec).

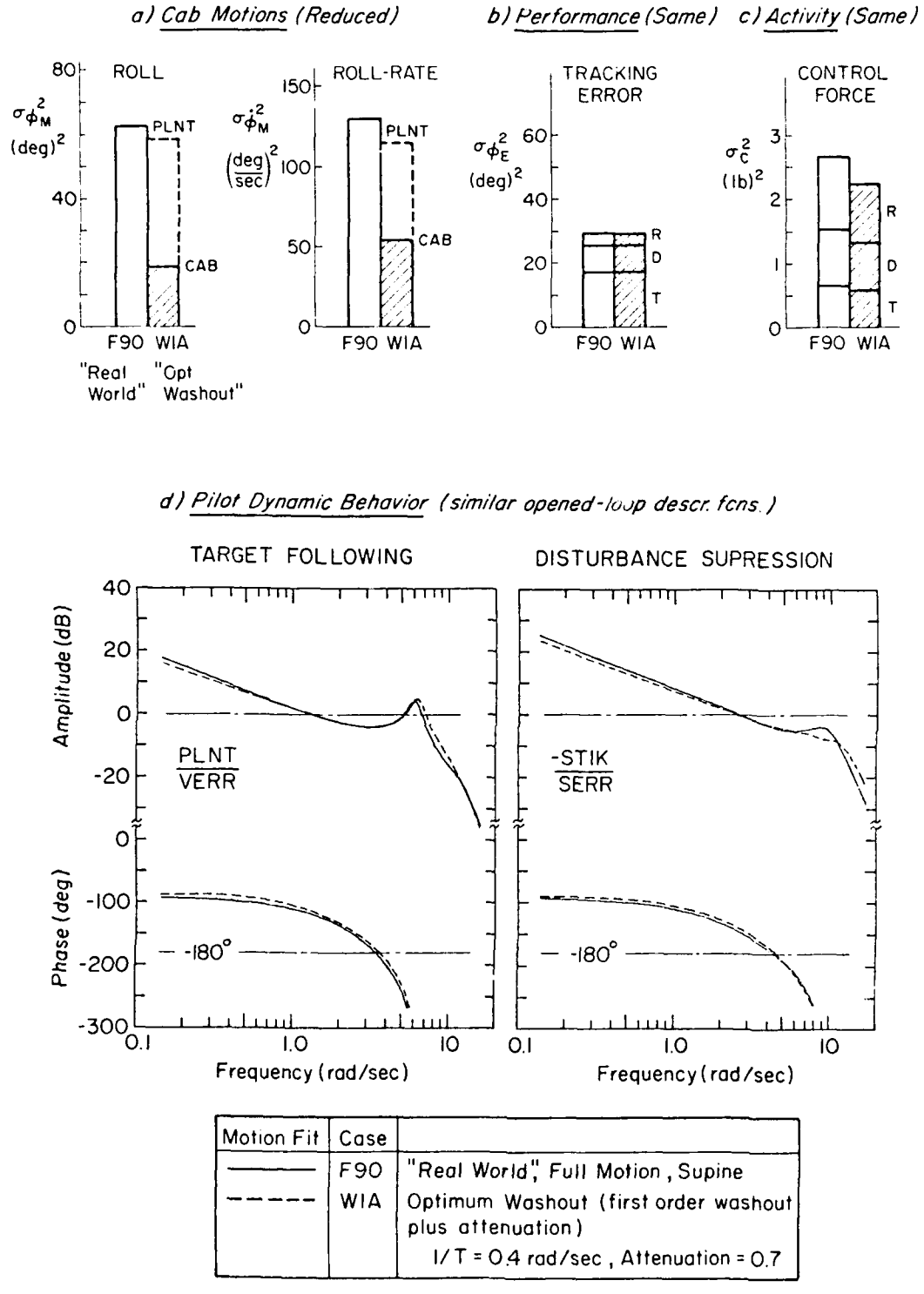

Figure 15. Comparison of Optimum Washout with "Real World" Case

CONCLUSIONS

Experiment I has covered several well-trained subjects' responses to a variety of motion cases in a roll-only motion simulator, with simultaneous target and disturbance inputs. The results support the following conclusions:

1) Across all seven conditions the four subjects were very consistent in their tracking behavior and scores, providing an exceptionally reliable and definitive data base worthy of detailed analysis, even beyond that described herein (e.g., on remnant effects).

2) The multiloop model structure presented in Figure 1, which has visual, motion, and common neuromuscular dynamic elements, proved capable of accurately fitting the closed- and opened-multiloop describing functions at all measurable signal points within the loop. In combination with the interleaved sum-of-sinusoids target and disturbance inputs, the new Multiloop Fitting Program (MFP) provided efficient fits of ten parameters in a strongly interacting multiloop situation. Such cases had heretofore been very difficult to fit because of the multiloop interactions involved between the visual and motion feedback paths.

3) Untangling the closed multiloop describing function data in the opened-loop manner shown here provides a ready comparison with traditional single open-loop data. Similar effects (e.g., the Crossover law adaptive behavior) are shown for the dual input case, with the disturbance loop having the higher bandwidth (limited mainly by the controlled element and vestibular rate sensing dynamics).

4) After the complex but consistent trends in the various cases have been digested, the key effects seem to be the following:

   - Given reasonable rate-motion cues at frequencies above about 0.5-1.0 rad/sec, the pilot's motion feedback system acts like an adaptive roll-rate damper with a bandwidth of nearly 3 rad/sec. This tends to suppress disturbances but opposes target-following motions, while stabilizing both loops.

   - The pilot then uses sufficient extra visual compensatory (error correcting) gain to follow target commands just as accurately under motion as in the static case, and with less remnant and disturbance components.

5) The effects of motion are consistent with the prior work of Shirley (1968), Stapleford et al. (1969), and Levison and Junker (1977). The new case covered here treats equally strong target and disturbance inputs, each having comparable spectra apparent at the display.

6) The describing functions and fitted tilt-cue parameter clearly showed that the spurious tilt cues from rolling with roll-axis horizontal are used, even though the rms lateral specific force was in some cases much less than 0.1 G_y. A very simple model for the use of this cue is given. Nevertheless, use of this cue resulted in only small improvements in tracking performance in this random-input tracking task, where large target roll angles are to be followed.

7) The four types of motion washout investigated (second-order, first-order, first-order-attenuated, and purely attenuated) showed distinct effects compared to the "real world" reference case of full motion about a vertical roll axis; the second-order case was the least desirable because of large differences in performance, behavior (describing functions), and subjective ratings. The other cases provided roughly similar performance measures among themselves with some small differences in relative remnant, describing functions, and ratings.

8) The pilots clearly adapted differently to the various washouts, thus complicating the job of predicting the net effects for a given washout.

9) The overall working hypothesis which emerges from these results is that the pilot uses primarily roll-rate cues in the vestibular sensitivity range (up to 3 rad/sec; about 0.5 Hz) as if he were an adaptive roll damper, then increases his visual target tracking gain to make up for the more sluggish responding pilot/aircraft inner loop which thereby results.

10) The optimum washout for roll-only simulators (from the standpoint of performance, behavior, and ratings similar to the "real world" reference case) was clearly the first-order attenuated washout. Recommended parameters (for this type of task) would be: attenuation factor 0.5-0.7, and washout time constant of 2-3 seconds (break at 0.3-0.5 rad/sec).

It would be interesting and fruitful to analyze and model the remnant portion of these data, using the closed-loop spectral data available (e.g., as in Figure 6). Because these inputs were carefully

selected and shaped to be representable by filtered white noise, various optimal control theories could be tested against this consistent, accurate, and definitive data base. Finally, using this model and these parameters (which precisely fit almost every data point), various analytical manipulations of the data can be performed to gain further insight about pilot adaptation to motion cues and washouts.

EXPERIMENT II — ROLL AND SWAY MOTIONS

BACKGROUND AND OBJECTIVES

Before describing the specific objectives of Experiment II, let us review the problem of simulating motions of aircraft involved in lateral maneuvers. Figure 16 shows some of the motion quantities involved in an idealized "turn entry" maneuver, wherein the pilot puts in a one second aileron pulse resulting in a 15 deg bank-and-stop maneuver. If the aircraft were well coordinated there would be no lateral specific force (LSF, apparent sideways acceleration on the pilot), i.e., the apparent net gravity vector would always parallel the pilot's spine. Vehicle acceleration caused by the banking of the lift vector would be nulled out by the aircraft accelerating to the right. The motions for free flight are shown by the dotted lines in Figure 16. The main problem for simulation is evident in the bottom of Figure 16; the simulator travel required to perfectly replicate free flight turns becomes excessive after a few seconds.

To alleviate this problem both roll and sway motion "washouts" are employed. First, the roll angle itself is gradually reduced to zero from the otherwise constant value that would be present in free flight. This is shown by the second plot in Figure 16, where a first-order washout filter reduces the bank angle from its peak with a time constant of T_ϕ = 2.5 sec = 0.4^{-1}. The resulting roll rate (the primary cue sensed by the pilot's vestibular system) is shown at the top. It can be seen that the rectangular roll rate pulse of the free flight case is distorted by this roll washout; it slightly reduces the main pulse and produces a spurious reversal in roll rate ("rate miscue").

In a roll-only simulator where no lateral travel of the cockpit is permitted (such as the DES in Experiment I), the pilot will also feel a false tilt cue given by $a_y \triangleq g \sin \phi$. Washing out the roll angle also reduces this false tilt cue.

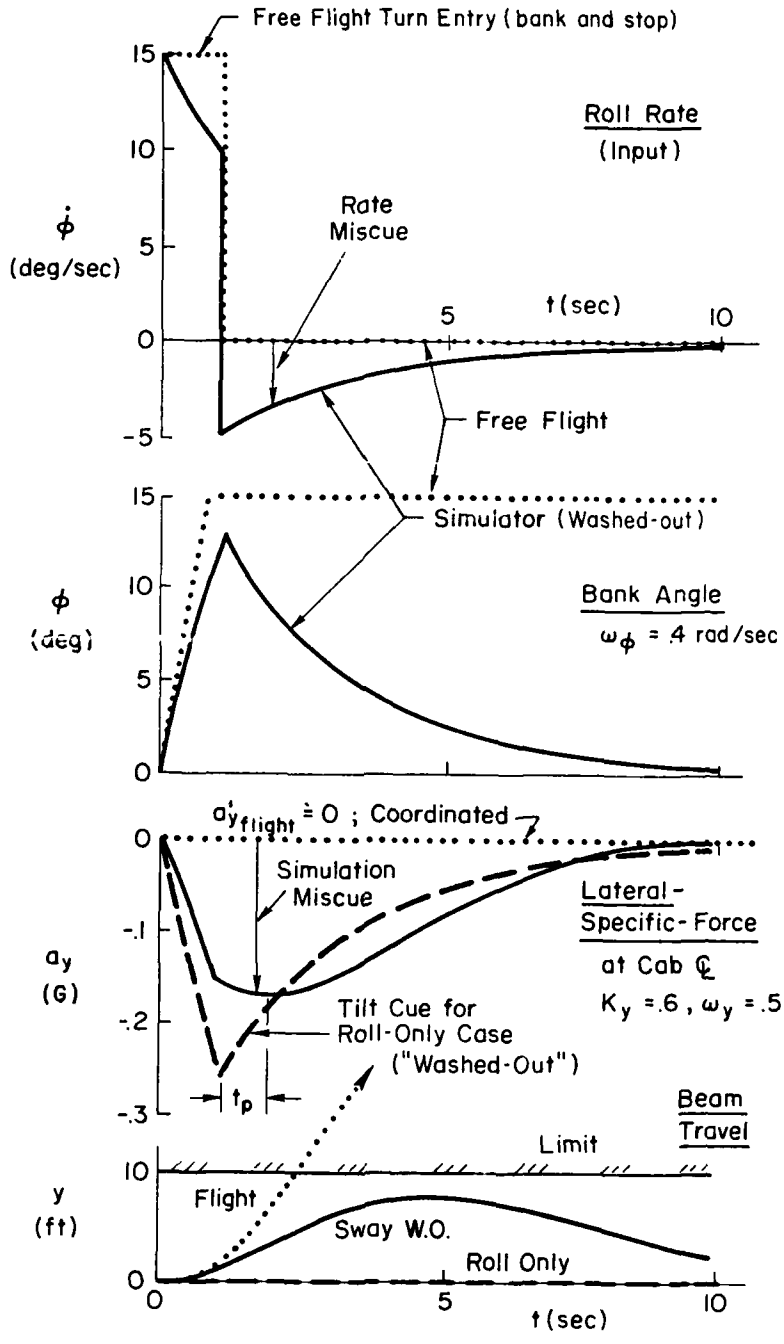

Figure 16. Comparison of an Idealized Turn-Entry in Free-Flight and a Motion Simulator Having Washed-Out Roll and Lateral Motions

Even with roll washout there remains some residual tilt cue, as shown by the dashed line in the third plot of Figure 16. This lateral-specific force can be further reduced by allowing the cab to accelerate laterally. However, even with the roll angle returning back to zero, as shown, the lateral travel required to remove all the LSF is excessive. Typically, the lateral motion (sway) drive also employs a first- or second-order washout to bring the cab back towards the center of the travel limits, about as shown at bottom of Figure 16. This limits the motion to just under 10 ft laterally and results in the LSF shown by the solid line in the plot above it. Two effects of sway washout are obvious from the a_y plot:

a) The peak miscue is reduced, as intended.

b) The peak of the a_y miscue is delayed relative to the pure tilt cue by t_p seconds.

These effects should be borne in mind when reading the rest of this report; for example, it turns out that the advantage gained by reducing a_y can be nullified by excessive delays of a_y with respect to the roll angle.

Even for this small maneuver, and with roll washout, the amounts of travel are large and require severe sway washouts to remain within the simulator limits. The sway washout does not reduce the miscue significantly over the roll-only case. Extremely large values of lateral travel (on the order of 50 to 100 ft) would have to be provided to reduce the LSF miscue to under 0.1 G for typical bank and stop maneuvers. Thus, the key problems addressed in this experiment were: what is the "least worst" sway washout that will (a) produce behavior as similar as possible to the free flight case and (b) produce miscues that are small enough to be acceptable by the pilots without seriously impairing the realism of the task.

Experiment I, discussed above, covered the roll-only washout case and found the opimum roll washout as one principal result. The current experiment extended the roll-only washout experiments performed on the DES to the case of both roll and "sway" motions and was performed on the LAMARS at AFFDL. The specific objectives included the following:

1) Perform tie-in runs to cross-validate the DES and LAMARS facilities, using comparable roll-only cases.

2) Compare experienced military pilots to the well-trained nonpilots used in Experiment I.

3) Investigate the effects of various types of sway washout to determine the acceptable limits, if any.

4) Investigate a nonlinear washout concept that showed promise in covering a large range of situations with one mechanization.

5) Correlate (to the extent possible) both objective effects on performance and piloting behavior with subjective evaluations of the motion cues felt by the pilots.

The results given in this paper cover these objectives roughly in the order given above.

APPROACH

The LAMARS (details discussed below under "Apparatus") is a large amplitude, five-degree-of-freedom motion system that allowed the DES task to be exactly replicated, in order to cross-validate both facilities, using the optimum washout case as the tie-in condition. Then, starting with this optimum roll-only washout the residual tilt error was reduced by various sway motions. By reshaping the target input spectrum it was possible to achieve perfect residual tilt coordination as one case, and a variety of sway washout attenuation and bandpass filter frequencies were also covered. These covered the range from subjectively barely noticeable to very distorting, to meet the objective of mapping out acceptable combinations of sway washout parameters.

The lengthy training required for nonpilots to achieve asymptotic roll tracking skills negated or even reversed any economic advantage over the case of off-duty military pilots. More important for Experiment II was the desire to have pilots evaluate the "realism" of turn entries with respect to actual flight. Thus, four experienced military pilots were found at AFFDL who could participate part time. They ran a

configuration and task identical to those of the former DES nonpilots, so that the scores and behavior (describing functions) could be compared between the two groups.

METHOD

Experimental Conditions

Control Task

The basic experimental task procedures and variables were similar to those used in Experiment I. The block diagram applicable to this experiment is shown in Figure 17, along with the relevant transfer functions. The basic task scenario was that of roll tracking in an air-to-air gunnery type encounter, wherein the target aircraft was performing evasive maneuvers which the pilot tried to track by matching his roll angle with that of the target. Simultaneously, there were unseen roll disturbances applied to the aircraft, such as those due to encounters with the tip vortices of the target aircraft.

Figure 17 shows that the "task" bank angle was subtracted from the target input to produce a compensatory tracking error displayed on the scope. This was given by a small aircraft-like symbol which only rolled (same as that of Experiment I in Fig. 2).

Controlled Element

Transfer functions* of various blocks in the diagram are shown in Figure 17. The controlled element was characteristic of a fighter having a neutrally stable spiral mode, a roll subsidence mode at 1.7 rad/sec, and an actuator mode of 5 rad/sec. With the DES simulator of Experiment I, a simulator drive mode having a frequency of 10 rad/sec

*In STI's shorthand notation for transfer functions, pure numbers are high-frequency gains; numbers in parentheses ( ) are first-order break frequencies; and numbers in brackets [ ] are damping ratio and frequency, respectively.

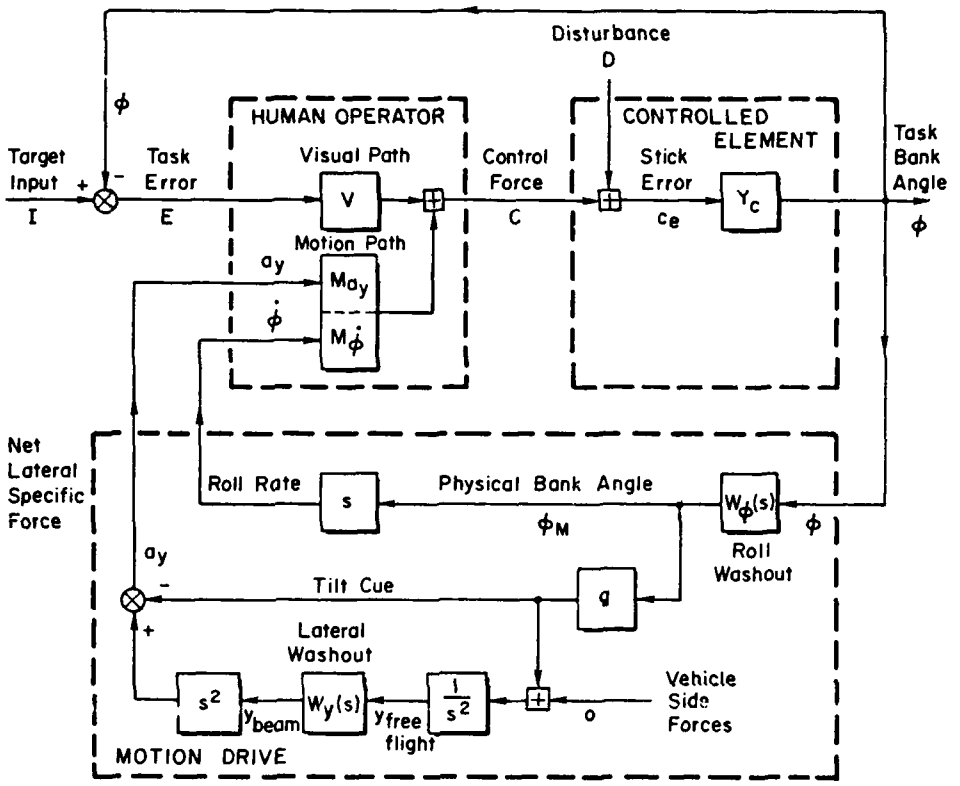

Controlled Elements:

"DES:"

$$Y_c(s) = \frac{\phi}{c} \doteq \frac{\overbrace{15000.}^{\text{Gain}}}{\underbrace{(0.)(1.7)(5.0)}_{(1/T)}\ \underbrace{[.37,\ 10.]}_{[\zeta,\ \omega]}} \quad \frac{\text{deg}}{\text{lb}}$$

or

"Smoothed":

$$Y_c(s) = \frac{\phi}{c} \doteq \frac{100.}{(0.)(1.0)(5.0)} \quad \frac{\text{deg}}{\text{lb}}$$

Roll Washout: (First-order)

$$W_\phi(s) = \frac{\phi_M}{\phi} = \frac{1.0(0)}{(.4)}$$

Lateral Beam Washout (Second-order)

$$W_y(s) = \frac{y_{Beam}}{y_{free\text{-}flt.}} = \frac{K_y(0)(0)}{[.7, \omega_y]} \quad \longleftarrow \text{Main Variables}$$

(↗ denotes adjustable parameters)

Figure 17. Block Diagram and Transfer Functions for Experiment II

and damping ratio of 0.37 was unavoidably present, and this is shown in the first controlled element denoted "DES." A second set of tests was made with these low-damped DES modes removed but with the roll subsidence modified to preserve roughly the same low-frequency characteristics. This is denoted by the "Smoothed" control element in Figure 17. The former was used to tie in the results with the previous DES experiments, while the latter was used to investigate the effects of the lateral beam washout.

Forcing Functions

Sums of seven (or eight) sinusoids, with amplitudes selected to approximate realistic target and disturbance spectra, were used for each quasi-random forcing function. As in Experiment I, the frequencies of the target and disturbance sinusoids were interleaved, such that disturbance input was mathematically uncorrelated with the target input. The provision of two such independent inputs enables both the visual and motion dynamics of the operator to be determined (see the discussion for Experiment I).

Two different inputs were used. The first, termed the "reference input," was identical to that used in Experiment I and contains large-amplitude, low-frequency roll motions which elicit significant tilt cues in the roll-only simulation. Cancelling these roll angles by sway motions required large lateral travel of the beam, so that a high amount of lateral beam washout had to be used in order to keep the beam within limits. Consequently, a "modified" input was employed, in which the low frequencies were attenuated to reduce the lateral travel requirements at any given level of beam washout. In effect, the input was washed out instead of the output. The modified input is tabulated in Table 5 as well as the shape of the "input washout" filter, Y_{iwo}.

Washouts

To tie in with the prior DES experiments a number of roll-only runs were made which had no roll washout. However, because residual tilts caused drifting of the beam under minimum beam washout conditions, some

TABLE 5

MODIFIED INPUT SPECTRA

TARGET (rms = 7.1 deg)			DISTURBANCE (rms = .74 lb = 3.4 N)		
Cycles / Run Length*	ω (rad/sec)	A_{dB} 0=1. deg	Cycles / Run Length	ω (rad/sec)	A_{dB} 0 = 1. lb
5	0.19	-15.1	9	0.35	-39.2
13	0.50	-0.7	17	0.65	-29.6
23	0.88	4.5	30	1.15	-15.5
37	1.42	4.7	49	1.88	-11.7
63	2.42	0.9	83	3.18	-9.7
107	4.10	-5.8	141	5.41	-9.2
182	6.98	-14.4	241	9.24	-10.0
309	11.85	-24.4	410	15.72	-11.7
SHAPING FILTER FORMS					
$\frac{1}{(s + 0.5)(s + 1.7)(s + 5.0)} \times Y_{iwo}$			$\frac{s}{(s + 0.5)(s + 5.)} \times Y_{iwo}$		

* Run length = 163.84 sec = 2.73 min

where "iwo" denotes "input washout."

$$Y_{iwo} = \frac{s^2}{s^2 + 2(.7)(1.)s + 1^2}$$

roll washout was necessary for the remainder of the runs. Based on the results given in Experiment I, we selected a 0.4 rad/sec first-order filter roll washout.

As shown at the bottom of Figure 17, the lateral beam washout was a second-order high-pass filter, i.e., constant acceleration inputs resulted in a constant position output, and a constant rate input resulted in a centered output of the beam. The break frequency, ω_y, was varied from the minimum washout condition of about 0.2 rad/sec up to and above 1.0 rad/sec, which approaches the bandwidth of the closed-loop maneuvers. The damping ratio was held constant at 0.7. The washout filter also had an attenuation factor, K_y, which reduced the high-pass level of the beam accelerations from 1.0 down to 0.20. The various combinations of K_y and ω_y will be given later.

In another set of runs a nonlinear mechanization was employed, which varied ω_y as an adaptive function of the roll angles and computed beam states, such as to maintain the minimum degree of sway axis washout consistent with the anticipated lateral motions. Further details on the nonlinear sway washout are given in the appendix herein and by Jewell and Jex (1979).

Many of the washout parameters that are shown in later tables as fixed variables in the experiment were first investigated by exploratory techniques, i.e., K_y and ω_y were varied in systematic and random manners, to map out the boundaries of subjectively noticeable effects. Such data are highly variable, interactive, and very difficult to average and to present in a systematic manner. Nevertheless, much of the effort of the simulation had to go into exploratory runs, in order to reduce the number of parameters to those formally tested. To accomplish this, adjustable (analog) washout filters were used in lieu of the normal LAMARS digital drive logic, and special operating techniques were evolved to permit their on-line adjustment.

Apparatus

The current experiment was performed on the USAF Flight Dynamics Laboratory's Large Amplitude Multimode Aerospace Research Simulator (LAMARS) at Wright-Patterson AFB, Ohio. The LAMARS has five degrees of freedom: heave, sway, roll, and (limited) yaw and pitch angles, provided to a one-man cab. The cab, mounted on a 20 ft cantilevered beam, can move vertically or horizontally through ±10 ft with compensating yaw and pitch motions such that it remains straight and level. High-performance servo drives are provided ("flat" bandwidth to roughly 3-4 Hz with about 0.7 damping ratio). The target was projected on the display screen with the same visual angle and shape as in Experiment I (Fig. 2). The roll motions were centered about the pilot's pelvis, instead of his head as in Experiment I. An overview of the development of the LAMARS is given by Hass et al. (1973).

Subjects

Experienced military pilots were used as subjects. Three of the four had experience as instructors in various types of military aircraft, and all had time both in fighters and heavier aircraft. Although these pilot subjects were not trained test pilots, they brought extensive experience in the real flight situation to the simulation, a perspective that was missing in the non-pilots tested previously in Experiment I. Therefore, these pilots could give commentary on the realism of each simulation case.

Procedures

Training and Data Collection Sequences

The pilots were given several sessions to train on the LAMARS simulator, in the various tasks. Because of their prior flight experience each reached asymptotic performance in only three to four sessions of about 1 hour each. Training was mainly on roll-only with reference input.

After training, the experimental procedures were generally as follows. In Session 1 the pilot was allowed a warmup run and then did the roll-only (tie-in with DES) runs, and the pilot was led through the various degrees of lateral beam washout. If the pilot could accept the range of washouts that had been previously established for other pilots, he was then run through a more formal set of runs in Session 2 in which describing function data were recorded, along with his subjective comments. In almost every case two or more runs were possible at each condition. The data were so consistent that further runs were felt to be unnecessary. Instead, the nonlinear washout runs were inserted as a third session for each pilot.

Table 6 shows the various combinations and sequencing of control element, input, and sway washout used in the LAMARS experiment.

The amount of sway washout shown varies from "none" (typical of free flight) through "low," "medium," "nonlinear" (similar to the medium washout) and "high" washout. "High" washout is only slightly different from a roll-only case (no sway motion), while for the "static" case there is no motion at all. The tradeoff between travel requirements and miscues is noted at the bottom of Table 6. The several variables mentioned above could result in an excessive number of test combinations, but this was avoided by making selected comparisons, as shown by the circled "cases" shown in Table 6. In effect, these comparisons investigated these subexperiments within the larger plan.

1) Tie in with previous DES experiment. Case (1) was run with identical control elements to the prior DES experiment, the only difference being the use of experienced pilots.

2) Controlled element effects. Case (9) was run with the "Smoothed" control element more typical of real aircraft to compare its results with the distinctive DES dynamics. A Static (no motion) Case (S) was run with the Smoothed Y_c, as one anchor point.

3) Sway effects. Comparisons of Cases (7) and (9) show the effects of sway motion with a medium washout, as required to maintain lateral sway travel within limits. It was not possible to compare a "no washout" case with the reference input because the lateral travel would have to exceed 160 ft.

TABLE 6. EXPERIMENT CONDITIONS

PLANT Y_c	INPUTS Φ_{TT}, Φ_{DD}	ROLL WASHOUT FREQ. ω_ϕ (rad/sec)	AMOUNT OF SWAY WASHOUT						
			NONE	LOW	MED.	N.L.	HIGH	ROLL ONLY	STATIC
			$K_y = 1.0$ $\omega_y = 0$ "FREE FLIGHT"	1.0 .25	.6 .5	.6 .2 ↔ .8 NON-LINEAR	1.0 1.0	1.0 ∞	
"DES"	"REFERENCE"	0.0						Tie-in w/D.E.S. ①	
"SMOOTHED"	"REFERENCE"	0.4	σ_y = 160 ft		Nonlinear W.O. Case ⑦ ↔ ⑧			Y_c Effects ⑨	
"SMOOTHED"	"MODIFIED" (Reduced at low frequencies)	0.4	σ_y > 40 ft	③	Input Effects ⑥	Sway Effects	⑤	②	Ⓢ

Washout Amount

— MORE MIS-CUE →

← MORE TRAVEL —

4) Input effects. To allow a lower degree of sway washout the "modified" input described earlier was used. This reduced the idealized free flight motion from 160 down to 40 ft and allowed a smaller degree of washout to maintain the cab within simulator limits. Comparing Configuration (6) with (7) documented the effects of the change in input alone. Because the resulting effects of input shaping on the describing functions were negligible, this comparison will not be further discussed in this report.

5) Sway washout variations. These were the primary runs of the experiment. With the "modified input" a range of increasingly severe washouts could be used, corresponding to Cases (3), (6), (5), and (2), respectively.

6) Nonlinear washout. Comparison of Cases (7) and (8) allowed us to determine the effects of the nonlinear washout mentioned above on performance and subjective ratings.

Measurements and Data Handling

Among the objective data recorded were: the task roll errors and control activities, and various motion quantities. In addition, signals were recorded at various points in the loop from which the pilot describing functions in response to both visual and motion inputs could be computed. The data reduction program and procedures were the same as those used in Experiment I.

Data Analysis

Using the reduced describing functions, the data averaging and model fitting and parameter identification were performed using the same techniques and Model Fitting Program (MFP) described for Experiment I.

RESULTS AND DISCUSSION

Tie-In with DES Experiments

The first goal was to establish the validity of a LAMARS simulation of the previous DES experiments for the roll-only case. The same display, control stick, controlled element, and drive logic dynamics were used, as validated by describing function measurements. Figure 18 compares the principal results of this and prior data. (Only three of the

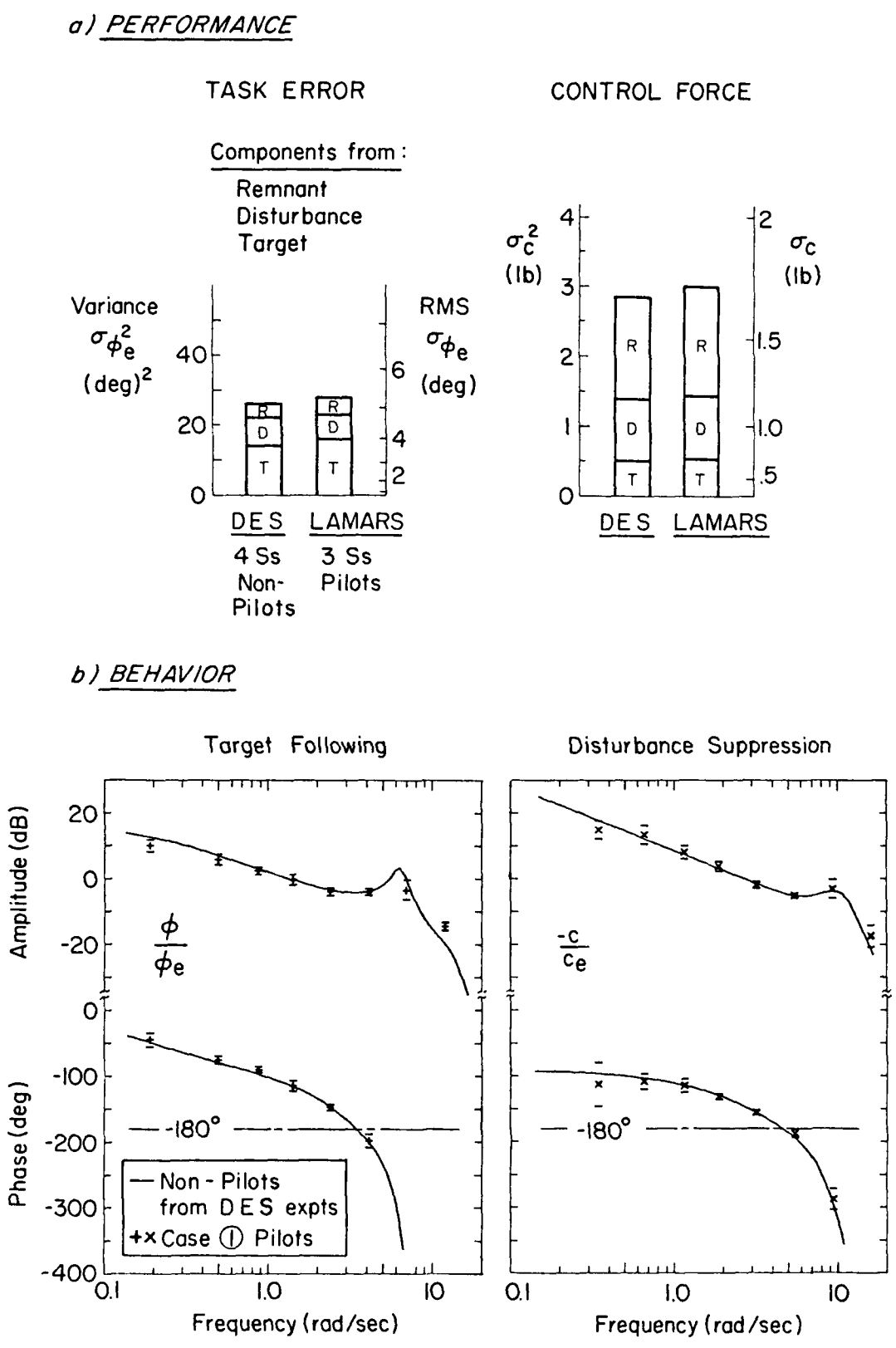

Figure 18. Results for Tie-In with Prior DES Experiments

four pilots completed these tie-in runs.) The performance results at the top present the variances of the task error and control force, along with their partitioning into target, disturbance, and remnant components. Remnant is the uncorrelated, or noise, portion of each signal. For convenience, an rms scale is also noted on the right side of each plot.

In both experiments, the magnitude and the partitions of performance measures were practically identical. The control-force remnant of roughly 40 percent is reduced to 15 to 20 percent in the error signal, because the controlled element filters the high-frequency remnant components.

The primary measures of pilot behavior are the two opened-loop describing functions for the simultaneously closed loops involved in target following and in disturbance suppression, as described under Experiment I. They are shown at the bottom of Figure 18. The points are from the present LAMARS experiments, as shown by the mean and standard deviations for the three pilots (at least two runs each). The low variability shows that all pilots followed the same behavior. The curve through the points is not a fit to these LAMARS data but is, in fact, the fit from the previous DES experiments with nonpilots. One could hardly expect a better fitting curve for the present data, and an independent MFP fit (not shown) gave nearly identical parameters. It is apparent that the three experienced pilots in the present LAMARS simulation adopted identical behavior and performance as that of the non-pilots in the previous DES experiments.

Because both the very well practiced nonpilots and experienced pilots adopted the same loop closures, we conclude that the behavior seen in both experiments was dictated by the combination of controlled element, input, and motion properties. This has two important implications:

- Roll motion experiments performed on the LAMARS may be reliably compared to those performed on the DES, thereby improving the breadth of coverage in basic research problems such as this.

- The DES could be used to train pilots or to perform preliminary experiments for the LAMARS, thereby reducing the total cost, because the DES is cheaper to operate than the LAMARS and may be more readily available.

The universality of pilot adaptation and performance demonstrated here gives further impetus to the proposition stated for Experiment I that valid control theory models of multiloop pilot behavior should closely match these results. All the inputs, controlled elements, and washouts are representable by simple pole-zero transfer functions, as can the pilot's behavior. The challenge is as follows: Can the optimal and/or classical models of pilot behavior replicate these results with a consistent set of cost functions and adjustment rules? The answers remain for users of this data base to resolve.

Pilot Versus Non-Pilot Training

It was found that the experienced pilots learned the task within a few sessions and achieved a fairly stable performance within a few dozen runs. There was a dramatic reduction from the training regimen which had to be used with the non-pilots in Experiment I (where hundreds of runs over a period of a few weeks were required to reach asymptotic performance). One implication of this observation is that the cost of non-pilots may not be much lower than of pilots, since the pilots require less practice to obtain stable performance levels.

Effects of Sway Motion

Figure 19 shows the effects of freeing the sway degree of freedom from roll-only (Case ⑨ vs. Case ⑦; both for the "smoothed" controlled element). At the top left, the sensed lateral specific force (LSF) is shown. In the roll-only case (which corresponds to infinite washout) the maximum spurious LSF reached 0.1 G_y, with peaks of 0.2 to 0.3 G. With lateral sway and medium sway washout, these peaks were reduced by about 20 or 30 percent. The achieved roll rate was practically identical, showing that the pilot used roughly the same high-frequency control actions. The sway travel was zero in the roll-only case and just under 4 ft in the medium case (occasional peaks to

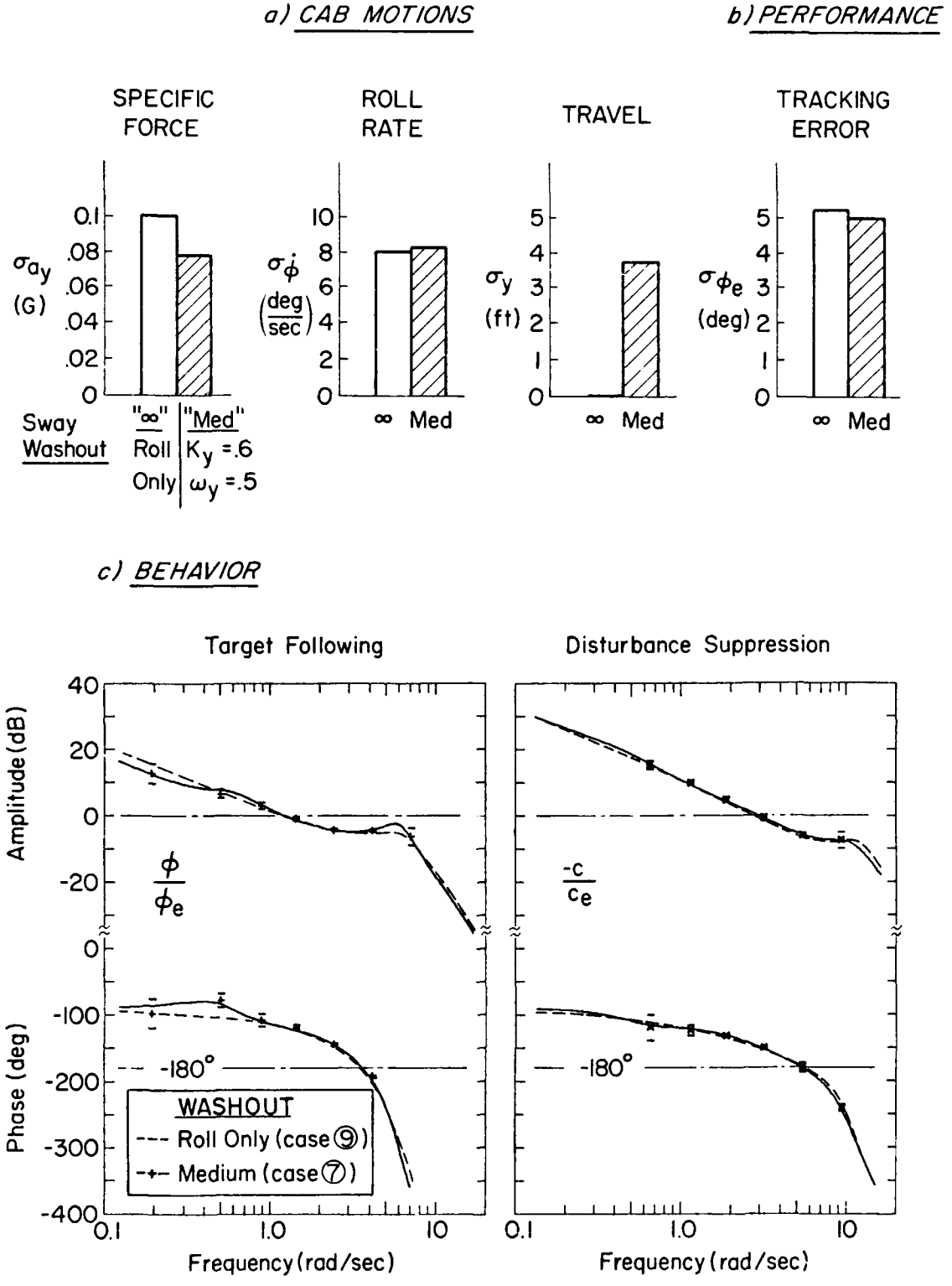

Figure 19. Effects of Washed-Out Sway vs. Roll-Only

10 ft). The tracking error performance was practically identical in both cases.

Figure 19c shows the effects of sway on the pilot control behavior. The dashed curve is that fitted to the roll-only data (not presented) for the smoothed control element. The solid curve is that fitted to the given data points using the Model Fitting Program described previously. The refined pilot model included: perception of both roll rate and roll accelerations, and LSF cues in the motion path, in addition to the classical pilot lead and time delays of the visual path and second-order neuromuscular dynamics. As in all of the DES and LAMARS cases analyzed to date, the curve fit to the data points is excellent, and the model clearly captures all the nuances of the measured describing functions.

Figure 19c shows two main effects of washed out sway motion in the describing functions:

- The disturbance control loop ($-c/c_e$) is essentially unaffected because neither the motion cues (which dominate $-c/c_e$ at high frequencies) nor the visual cues (which dominate at low frequencies) are affected by the medium washout.

- The target tracking loop (ϕ/ϕ_e) is only affected at low frequencies, where the lateral specific force cues give helpful tilt cues in the roll-only case, but are distorted and less effective in the washout case (as shown by the lower gain below ω = 0.5 rad/sec).

Overall, there is remarkably little difference in performance and behavior between the roll-only and the roll-plus-sway case, with this medium sway washout. One reason is that the washout did not remove much of the tilt cue, as shown by the similarity of LSF in Figure 19a. The pilot's subjective comments are discussed separately, later.

Effects of Various Degrees of Sway Washout

The main set of variables, in which ω_y and K_y were varied produced almost negligible changes in the specific measures of pilot performance and behavior. It had been expected that the wide range of sway washouts (which do result in adverse comments) would result in a behavioral

change, but this was not apparent from the data. In general, the describing function differences among the sway washout combination (Cases ③, ⑥, ⑤, and ②) were similar to the data separations shown in Figure 19. The one case with significant reductions in describing function gains, ③, was highly confounded by encounters with soft stops (travel limiters), hence no transfer function data will be presented.

Figure 20 compares various measures of motion output and performance among the various sway washouts tested, arranged in the same order of increasing severity as in Table 6. The second set of bars compares the lateral travel for the various washouts. As would be expected, the rms travel reduces from the untested (but calculated) value of over 40 ft for free flight to 3.3 ft (10 ft peaks) for the least sway washout that could be used, to further reductions to ≈1 ft (3-4 ft peaks) for the medium and high degrees of washout. The extent of travel is greatly reduced by the sway washout, as was expected.

The first set of bars shows that the spurious lateral specific force cue increases with washout severity, also as expected. The rms levels of this LSF are quite low, with the peaks (≈ 3σ) reaching values of only 0.1 G for the medium, high, and roll-only cases. The basic tradeoff between travel and miscue is clearly apparent from these data: one obtains reduced travel at the expense of increased miscues.

Looking now at the bottom of Figure 20 for measures of the tracking performance and behavior, one sees that the roll rate was practically identical among all sway washouts. This means that the roll loop was closed in the same manner, regardless of the presence of the (often subthreshold) LSF cues. In other words, lateral specific force cues were essentially ignored in the roll loop closure.

The same conclusion applies in the roughly equal tracking errors and control force measures at the bottom of Figure 20. These performance measures cannot be considered to be the whole story because the pilot's subjective comments differed significantly among these various washouts, as will be discussed later.

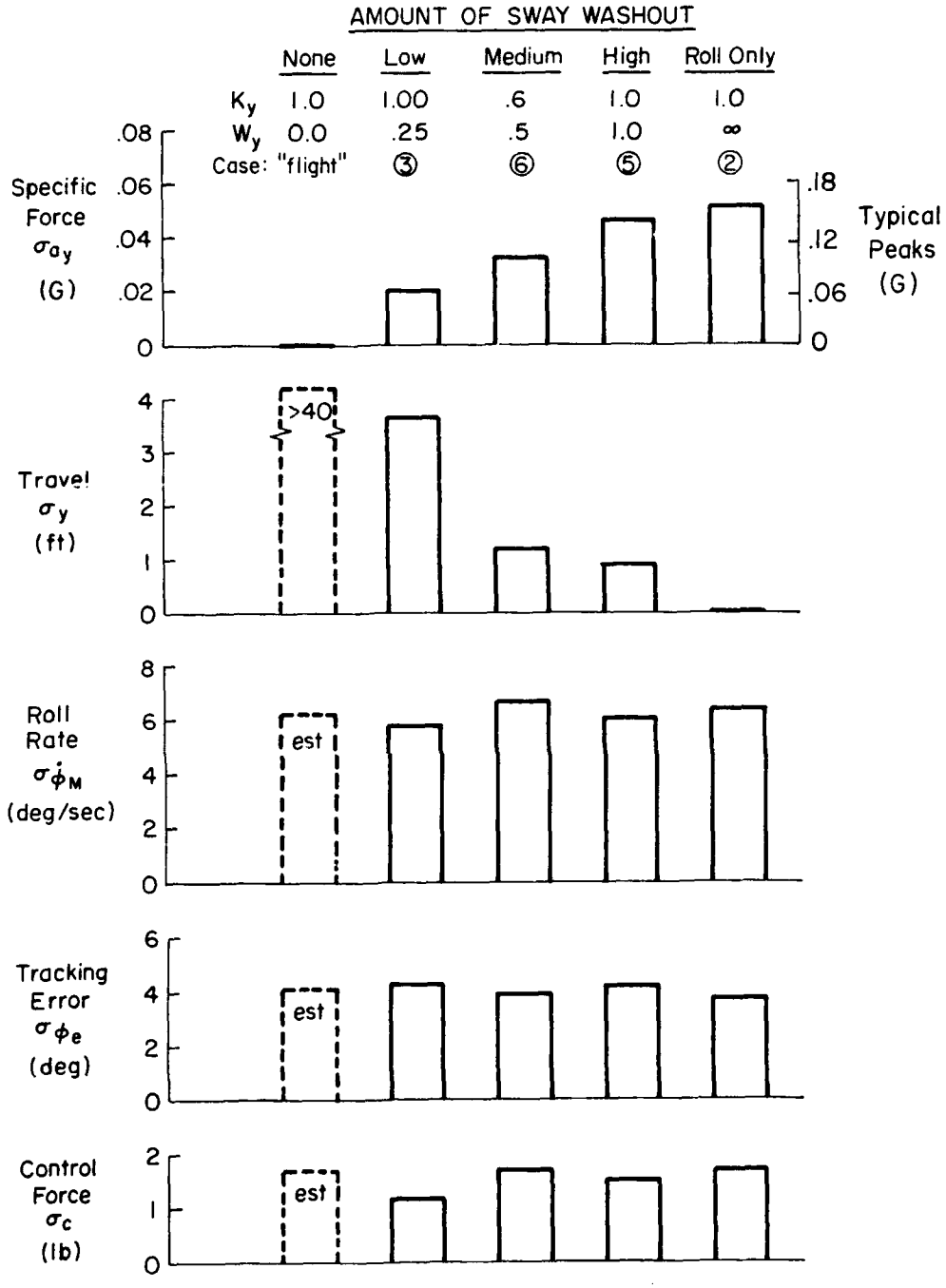

Figure 20. Comparisons Among Various Sway Washouts

A word of caution is in order here, as it might be inferred that, if reliable behavior can be obtained with roll-only simulation, considerable expense (in terms of lateral motion systems) could be saved by eliminating the sway motions. However, lateral specific forces are often simulated for other purposes, such as roll-yaw coordination (e.g., for rudder use, engine-out effects, or direct side force simulation), so roll-only simulation is not a panacea for the general case.

Another problem was hinted at during these tests — that of possible negative transfer of training from the roll-only case (wherein a rightward-tilt requires a left aileron correction) to the free-flight case (where the corresponding leftward LSF in general would not result in a left aileron correction). Evidence of this reversal effect was present when the sway degree of freedom was turned on, so the roll-only runs were discontinued as warmups for the sway washout sessions. This negative transfer effect bears further study.

Linear Versus Nonlinear Washout

A nonlinear washout algorithm was evolved which would automatically adjust the sway washout filter frequency, as a function of the sway command states, as well as the proximity to the sway limits. Soft limiting of large excursions can only be obtained by the addition of LSF miscues, and it was the basic question of this comparison to see whether the decelerations for a large motion would be acceptable to the pilot. The nonlinear algorithm keeps the washout as low as possible during low roll motions, and increases it only as much as is necessary to cope with large roll motions. Consequently, one algorithm could be used for a large number of conditions, instead of having to "optimize" the sway washout parameters for each condition, as is necessary with fixed sway washouts. The mechanization is described in the appendix and in Jewell and Jex (1979).

Figure 21 depicts the results of comparing the nonlinear with the "medium" washout, which it approaches for small motions. The larger reference input was used to maximize the sway cues. The bar charts for cab motions show that the lateral specific force, roll rate, and lateral

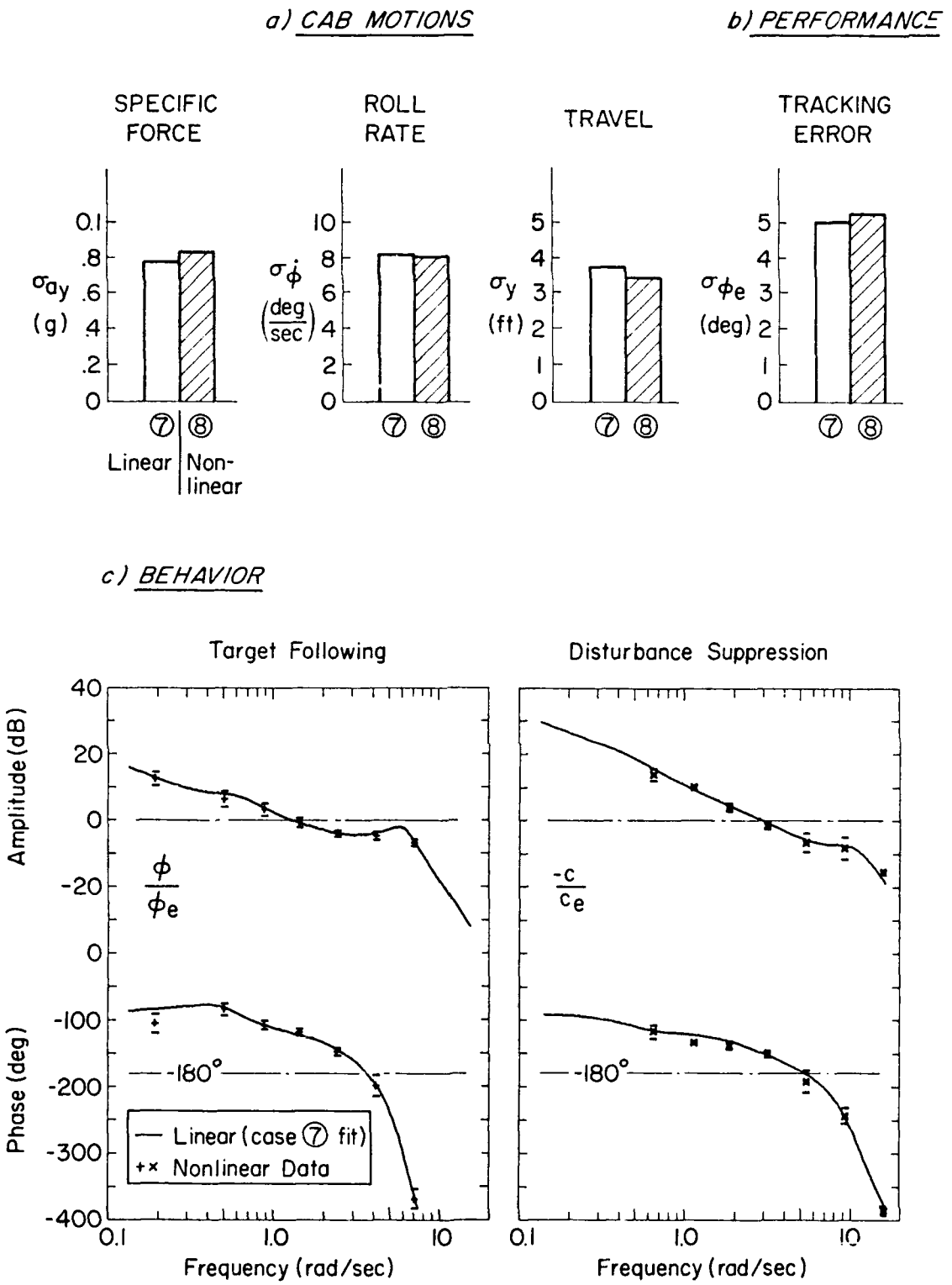

Figure 21. Comparison of Linear and Nonlinear Washouts

travel were practically identical for either case. What is not shown here is that the nonlinear washout case (shown shaded) resulted in fewer bumpings of the parabolic limiters than did the linear case. When the cab encounters the parabolic limiters, large braking forces are put in, and the yaw rate coordination mechanism of the cab is ineffective. The pilots reported a tendency to become disoriented after such encounters. These incidents were greatly reduced in the nonlinear washout case, which the pilots liked. On the other hand, the adaptive circuitry puts in slightly higher centering decelerations (which are miscues, per Figure 16).

The tracking error plot shows that the performance was practically identical in either case. Figure 21c gives the transfer functions comparing the fitted curve for the linear case (Case (7)), with the nonlinear data of Case (8) showing practically identical behavior. (A linear model fit for the nonlinear data is not strictly applicable because of the time variation in the washout properties.) Nevertheless, it can be seen that the linear case curve fits the nonlinear case data quite well, implying essentially identical behavior.

These results suggest that the nonlinear sway washout is a promising way to economize on experimental operations because the algorithm seems to work over a large range of inputs. A number of discrete (i.e., bank and return) and other input cases were checked with the nonlinear washout during this experiment. In all cases the results seem to be similar to those shown. We recommend this nonlinear sway washout scheme for other simulators having similar travel limits.

Subjective Evaluations

Although a great deal of pilot commentary was taken during these experiments, it was difficult to establish firm correlations with the washout parameters. The motions, although noticeable, did not strongly affect the pilot's control strategy, and in many cases the LSF involved was small enough to be almost "subthreshold." It turned out that this LSF threshold effect was the dominant distinguishing feature between cases which could be consistently evaluated and in cases which were

vaguely and inconsistently evaluated. As noted earlier in Figure 20, the peak LSF were under 0.05 G for the reduced input cases and approached 0.10 for the reference input cases. The peak LSF did vary somewhat more than this due to occasional large motions; this enabled the pilot commentaries to be made when they occurred. In many of these cases the pilot was also allowed to make bank-and-return maneuvers within the confines of the simulator. In such cases the lateral specific forces often exceeded 0.1 G, so the sway washout effects became more readily apparent.

Accordingly, we have plotted the peak LSF versus the washout filter frequency (ω_y) and washout attenuation factor (K_y) on Figures 22a and 22b, respectively. Along with each of the data points is given the consensus of comments among the pilots. First, notice the black points which are those obtained during the roll tracking cases with reduced inputs. The peaks seldom exceeded 0.1 G, and the general consensus of pilot comments was vague. Only for very low values of K_y in Figure 22b (which correspond to roll alone) did the LSF exceed 0.1 G, and there was some comment about noticing the tilt cue or the "leans."

Considering next the open symbols for the rapid bank and return maneuvers, it can be seen that when the lateral specific force peaks exceed about 0.1 G there were distinct comments that had some correlation with the task variables. (Crossplots of these effects will be shown later.)

It is inferred from careful study of these runs and related comments that, when lateral specific force peaks lie below about 0.1 G, the LSF effects are at best only vaguely perceived, and at worst are inconsistent. This hypothesis may help explain some of the apparently inconsistent results from other investigators, where the lateral specific force peaks are known to have been less than 0.1 G (e.g., Shirley, 1968; Stapleford et al. 1969). Others (e.g., Sinacori, 1978; Hofmann and Riedel, 1979) have suggested that such an "indifference threshold" should be operational on lateral specific force cues. More recently, Roark and Junker (1980) have shown that the threshold of detectable tilt

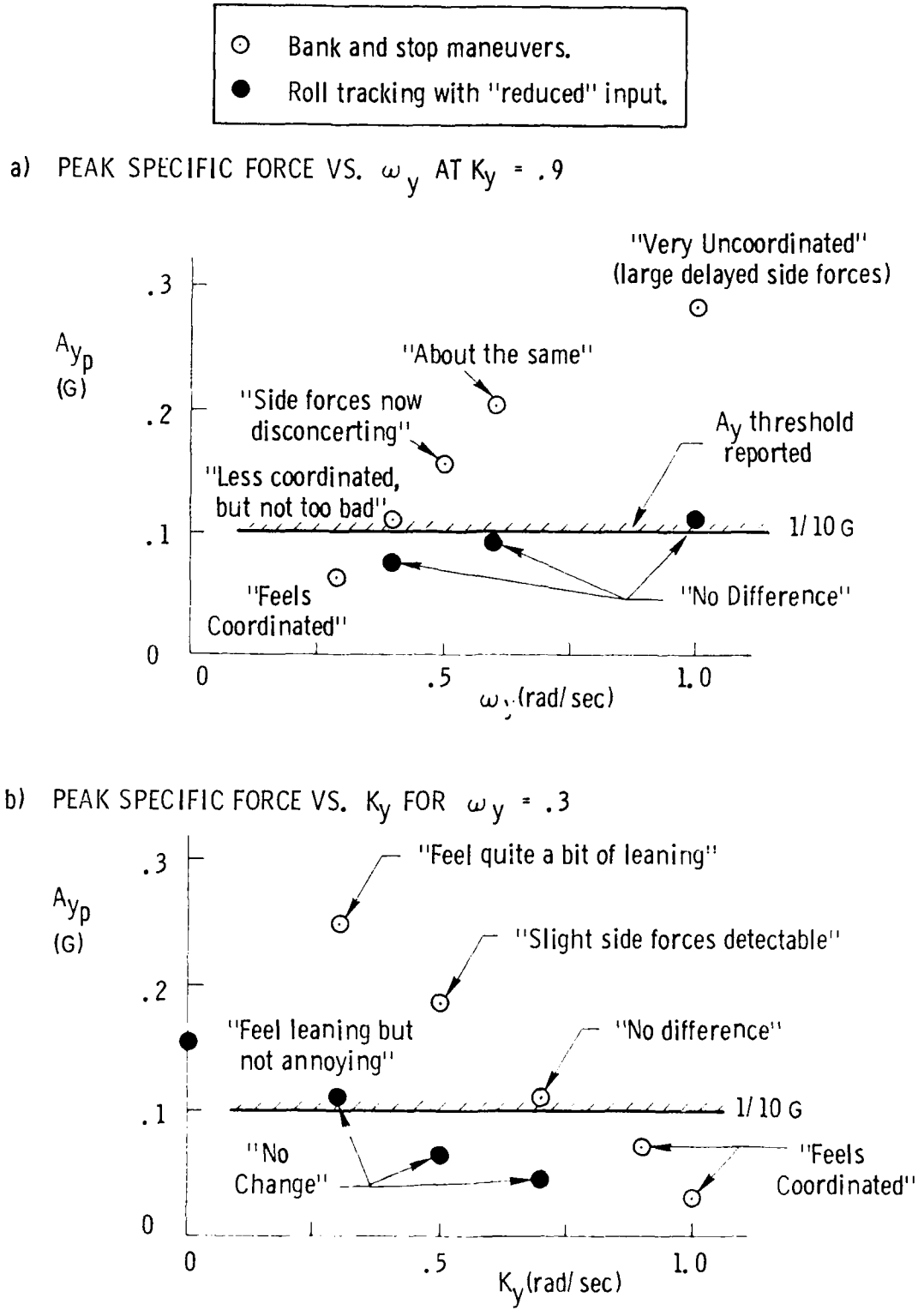

Figure 22. Peak Specific Force and Comments vs. Sway Washout Frequency and Gain

cues is about 4-9 deg (0.07-0.15 G_y), while tracking. Our data agree with their findings.

The findings have important consequences for the design and interpretation of experiments involving lateral motions. If the expected LSF cues are less than 0.1 G, the experiment may be expected to encounter confused pilot commentary. If the small cues are used in important ways for coordination and for detection of certain types of failure, then such small levels might be worth investigating. On the other hand, if the lateral specific force cues are greater than 0.1 G, they will surely be noticed and used, and if they are due to motion-base artifacts they may affect the results in a negative manner.

Gathering and sifting those cases where the motion cues were strong enough to give significant commentary, the correlations shown in Figure 23 summarize the consensus from this experiment. Figure 23 represents a "subjective commentary map," wherein the coordinates are washout frequency along the abscissa and attenuation factor as the ordinate. The bottom left corner represents fully coordinated free flight. Regions of distinct subjective effects are denoted by the fuzzy boundaries and paraphrased comments.

It is noted that a good portion of the desirable washout parameters (values of K_y near 1.0 and $\omega_y < 0.2$ rad/sec) exceed the travel limits of the simulator. A barely acceptable region was observed for K_y = 0.3-0.6 and ω_y = 0.2-0.4 rad/sec, where the LSF miscues are small enough and the peaks are not unduly delayed with respect to the roll angles to cause apparent distortion.

Consider next the "leans" region (at the top of Fig. 23b) where the sway attenuation is reduced towards zero, implying no sway motion whatsoever. In these cases the motions approach roll-only, and the tilt cue is closely in phase with the roll angle. Hence, there is little confusion between the source of the lateral specific force and the observed roll angles. We call this syndrome of effects "the leans" because the pilots are aware that the perceived LSF is due to the spurious tilt cues.

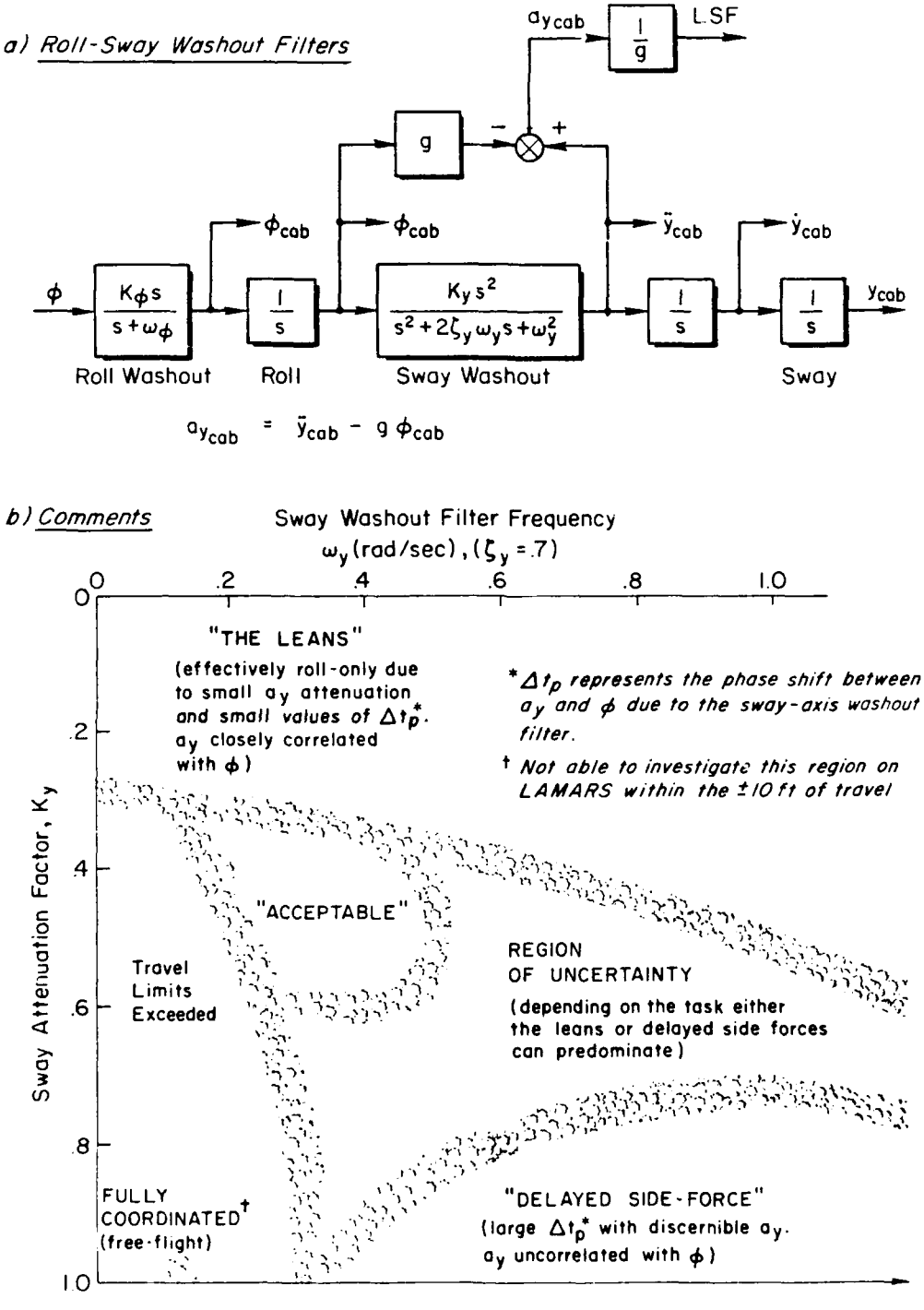

Figure 23. Correlations of Comments vs. ω_y and K_y

At the bottom right of Figure 23, the attenuation factor is nearly unity, high washout frequencies are present, and the "delayed side force" effect (noted earlier in Figure 16) was apparent. Here, the side force peak, even though small, was delayed with respect to the roll angle peak. This distortion seemed to cause disconcerting motion effects, because it is harder to assimilate into the pilot's experience with aircraft. Finally, at the right center there is a large range of undesirable properties where the washout filter frequencies are on the order of 1.0 rad/sec and attenuation was large (K_y = 0.5-0.9), which produced highly distorted lateral motion cues. In several runs the pilots claimed that the spurious cues were like those of a student pilot putting improper inputs into the rudder pedals. The obvious conclusion from Figure 23 is that it is difficult to achieve an acceptable degree of washout within the ±10 ft confines of the LAMARS. This conclusion is not inconsistent with experience of other aircraft simulations both on the LAMARS and elsewhere. So much landscape is required to reduce the spurious lateral specific force cues below 0.1 G that acceptable sway simulation can seldom be afforded in a practical simulator.

CONCLUSIONS

The following conclusions are drawn from Experiment II:

1) There is an excellent tie-in between the Dynamic Environmental Simulator and the LAMARS simulations when the same roll-only cases are simulated.

2) The military pilots of Experiment II and trained non-pilots from Experiment I showed nearly identical behavior and performance, implying universality of adaptation and results. However, the pilots needed much less training time than the non-pilots due to their previous flight experience. This emphasizes one advantage of using actual pilots in such basic research — the amount of training time necessary to obtain valid results can often be reduced by an order of magnitude when real pilots are used, thereby offsetting their scarcity and expense.

3) Both step and random tracking gave rise to spurious lateral motion cues (the turn-coordinated free-flight case would have none) which were fuzzily categorized as "out of phase," "like a student on the rudder pedals," etc. Analysis showed these to be roughly correlated by time- and frequency-response parameters related to K_y and ω_y.

4) Neither the roll tracking behavior nor error performance were significantly affected by a variety of lateral sway washouts.

5) Pilot comments were consistent only when the peak lateral specific forces exceeded about 0.1 G. Pilots noticed "leans" (tilt effects) and "delayed side forces" (delays between peak roll angles and peak side forces).

6) A nonlinear beam washout filter (working on computed sway states) reduced the rate of soft-stop encounters, at the expense of occasional, smooth lateral-specific-force (a_y) peaks, but otherwise did not affect behavior or performance. It promises to provide an adaptive washout which does not need to be "fine tuned" to avoid hitting stops while minimizing spurious washout artifacts. Additionally, it should be especially useful during training, where motion cue usage is changing.

7) These results imply that sway motions well over ±10 ft should be provided to reduce lateral motion miscues to acceptable levels wherever lateral specific force cues are of research interest.

It would be valuable to find and simulate exactly some real-world tasks in which the free-flight motions would be under ±10 ft, such as aerial refueling or shipboard VTOL landing. Our hypothesis would predict that unless the peak lateral specific forces would exceed 0.1 G (unlikely) the lateral motion cues would not be of significant value in the task, in that the pilot's dynamic behavior would be essentially unchanged.

APPENDIX

FUNCTIONAL DESCRIPTION OF THE NONLINEAR WASHOUT FILTER

Figure A-1 contains a functional block diagram of the roll-sway washout filters. The break frequency of the sway washout filter, ω_y, was programmed to vary, on-line, according to the following non-linear control laws:

$$\omega_{\bar{y}} = \int [c_y(\dddot{y} + \ddot{y} + \dot{y})^2 + (\omega_{y_o} - \omega_y)]dt \qquad \text{(A-1)}$$

and

$$\omega_y = \begin{cases} \omega_{y_{max}} & \text{for } \omega_{\bar{y}} > \omega_{y_{max}} \\ \omega_{\bar{y}} & \text{for } \omega_{y_o} < \omega_{\bar{y}} < \omega_{y_{max}} \\ \omega_{y_o} & \text{for } \omega_{\bar{y}} < \omega_{y_o} \end{cases} \qquad \text{(A-2)}$$

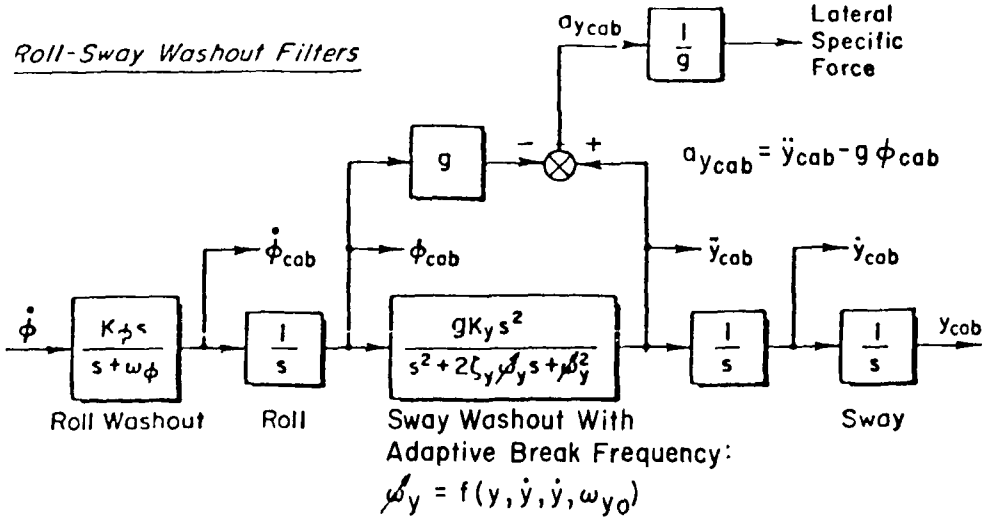

Figure A-1. Functional Block Diagram of the Nonlinear Roll-Sway Washout Filters

The integration in Eq. A-1 is held up when ω_y' exceeds any of the limits defined in Eq. A-2.

The rationale behind varying ω_y as described above is to increase the constraint against the lateral movement of the simulator as its predicted position moves farther away from the center position. The procedure can be thought of as a centering spring with a variable spring constant. Earlier versions of this nonlinear washout approach were reported by Parrish (1975).

The values of the parameters in Eqs. A-1 and A-2 can be set based on the physical limits of the simulator (maximum roll angle, ϕ_{max}, and lateral sway, y_{max}), and the values of K_ϕ and K_y (see Fig. A-1). Expressions for $\omega_{y_{max}}$ and c_y are presented below without proof.

$$\omega_{y_{max}} = \left[gK_\phi K_y \frac{\phi_{max}}{y_{max}}\right]^{1/2} \qquad \text{(A-3)}$$

$$c_y = \omega_{y_{max}}/y^2_{max} \qquad \text{(A-4)}$$

The value of ω_{y_o} should be set to some small positive value (e.g., less than 0.1 rad/sec) such that negligible sway phase distortion occurs at crossover frequencies near 1 rad/sec. The nominal values for these parameters for the experiments described in this report were:

$$\omega_{y_o} = 0.050 \text{ rad/sec}$$

$$c_y = 0.010 \text{ rad/ft}^2\text{-sec}^2$$

$$\omega_{y_{max}} = 0.50 \text{ rad/sec}$$

REFERENCES

Ashkenas, I. L., H. R. Jex, and D. T. McRuer, 1964, Pilot-Induced Oscillations: Their Cause and Analysis, NOR 64-143, Northrop Corporation, Norair Division, Hawthorne, California.

Hass, R. L., H. E. Hotz, and G. R. Mills, 1973, "The Large Amplitude Multi-Mode Aerospace Research (LAMAR) Simulator," AIAA Paper 73-922, presented at AIAA Visual and Motion Simulation Conference, Palo Alto, California.

Hofmann, L. G., and S. A. Riedel, 1979, Manned Engineering Flight Simulation Validation. Part I: Simulation Requirements and Simulator Motion System Performance, AFFDL-TR-78-192 (AD A-071394), Air Force Flight Dynamics Laboratory, Wright-Patterson Air Force Base, Ohio.

Jewell, W. F., and H. R. Jex, 1979, A Second Order Washout Filter with a Time-Varying Break-Frequency, WP-1094-9, Systems Technology, Inc., Hawthorne, California.

Levison, W. H., S. Baron, and A. M. Junker, 1976, Modeling the Effects of Environmental Factors on Human Control and Information Processing, AMRL-TR-76-74 (AD A-030585), Aerospace Medical Research Laboratory, Wright-Patterson Air Force Base, Ohio.

Levison, W. H., and A. M. Junker, 1977, A Model for the Pilot's Use of Motion Cues in Roll-Axis Tracking Tasks, Rept. 3528, Bolt Beranek and Newman Inc., Cambridge, Massachusetts.

Magdaleno, R. E., and R. W. Allen, 1975, Modeling Biodynamic Effects of Vibration, AFOSR 75-1236 TR (AD A-073819), Air Force Office of Scientific Research.

McRuer, D. T., and E. S. Krendel, 1974, Mathematical Models of Human Pilot Behavior, AGARD-AG-188, North Atlantic Treaty Organization, Advisory Group for Aerospace Research and Development.

Parrish, R. V., J. E. Dieudonne, R. L. Bowles, and D. J. Martin, Jr., "Coordinated Adaptive Washout for Motion Simulators," J. Aircraft, Vol. 12, No. 1, Jan. 1975, pp. 44-50.

Roark, M., and A. M. Junker, 1978, "The Effects of Closed-Loop Tracking in a Subjective Tilt Threshold in the Roll Axis," in Proceedings of Fourteenth Annual Conference on Manual Control, NASA CP-2060, National Aeronautics and Space Administration, Washington, D.C.

Shirley, R. S., 1968, Motion Cues in Man-Vehicle Control, Sc.D. Thesis, Massachusetts Institute of Technology, Cambridge, Massachusetts.

Sinacori, J. B., 1977, A Brief Survey of Motion Simulators' Drive Logic with Emphasis on the Roll Axis, WP-1094-2, Systems Technology, Inc., Mountain View, California.

Stapleford, R. L., R. A. Peters, and F. R. Alex, 1969, Experiments and a Model for Pilot Dynamics with Visual and Motion Inputs, NASA CR-1325, National Aeronautics and Space Administration, Washington, D.C.

Zacharias, G. L., and L. R. Young, 1977, "Manual Control of Yaw Motion with Combined Visual and Vestibular Cues," in Proceedings; Thirteenth Annual Conference on Manual Control; Massachusetts Institute of Technology; Cambridge, Massachusetts.

☆U.S.Government Printing Office: 1981 — 559-007/6007